AD-A131 156 PHASE CONJUGATION IN A RING LASER CAVITY(U) NORTH TEXAS 1/1
STATE UNIV DENTON CENTER FOR APPLIED QUANTUM
ELECTRONICS J M DIELS 30 JUN 83 N00014-81-C-0816
UNCLASSIFIED F/G 20/5 NL

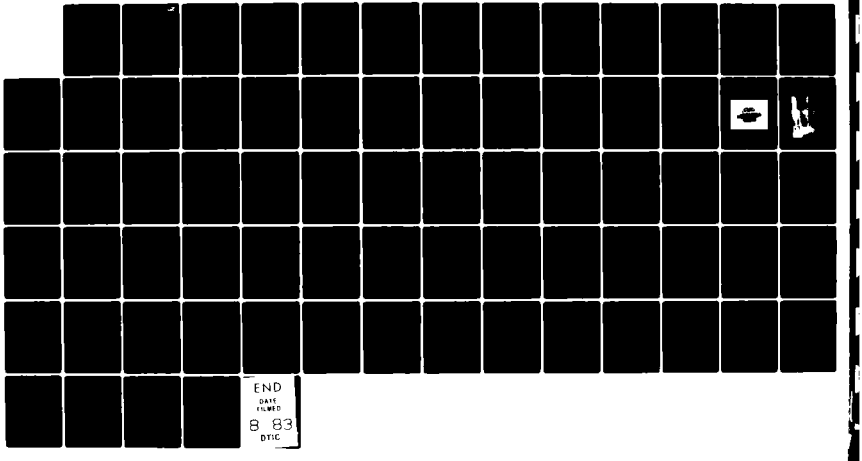

END
DATE FILMED
8 83
DTIC

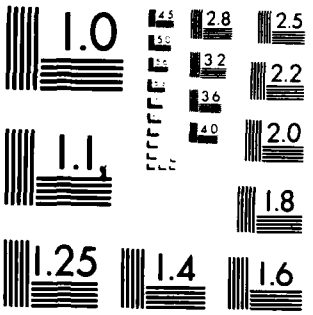

MICROCOPY RESOLUTION TEST CHART
NATIONAL BUREAU OF STANDARDS-1963-A

UNCLASSIFIED

SECURITY CLASSIFICATION OF THIS PAGE (When Data Entered)

REPORT DOCUMENTATION PAGE

READ INSTRUCTIONS BEFORE COMPLETING FORM

1. REPORT NUMBER
2. GOVT ACCESSION NO. AD-A131156
3. RECIPIENT'S CATALOG NUMBER

4. TITLE (and Subtitle)
Phase Conjugation in a Ring Laser Cavity

5. TYPE OF REPORT & PERIOD COVERED
Final - 9/1/79 to 8/31/82
(+ 6 month extension)

6. PERFORMING ORG. REPORT NUMBER
N/A

7. AUTHOR(s)
Jean-Claude M. Diels

8. CONTRACT OR GRANT NUMBER(s)
N00014-81C-0816
(N00014-79C-0947)

9. PERFORMING ORGANIZATION NAME AND ADDRESS
Center for Applied Quantum Electronics
North Texas State University, Box 5368
Denton, Texas 76201

10. PROGRAM ELEMENT, PROJECT, TASK AREA & WORK UNIT NUMBERS

11. CONTROLLING OFFICE NAME AND ADDRESS
Office of Naval Research
Physics Division Office
Arlington, Virginia 22217

12. REPORT DATE
June 30, 1983

13. NUMBER OF PAGES
72

14. MONITORING AGENCY NAME & ADDRESS(if different from Controlling Office)

15. SECURITY CLASS. (of this report)
UNCLASSIFIED

15a. DECLASSIFICATION/DOWNGRADING SCHEDULE

16. DISTRIBUTION STATEMENT (of this Report)
Approved for public release, distribution unlimited

17. DISTRIBUTION STATEMENT (of the abstract entered in Block 20, if different from Report)

18. SUPPLEMENTARY NOTES

19. KEY WORDS (Continue on reverse side if necessary and identify by block number)

20. ABSTRACT (Continue on reverse side if necessary and identify by block number)

We investigate the dynamics of phase conjugation by degenerate four wave mixing (DFWM) inside a laser cavity. This problem is shown to be important in connection with (a) protection of a high power laser against self focusing and (b) development of a new type of laser gyro. Our theory demonstrates that fast optical and temporal phase conjugation by DFWM is incompatible with large ($\simeq 1$) reflection coefficients. Therefore, it appears to be better to implement DFWM for the coupling of the two counterpropagating pulses in a ring

DD FORM 1 JAN 73 1473 EDITION OF 1 NOV 65 IS OBSOLETE
S/N 0102-LF-014-6601

UNCLASSIFIED
SECURITY CLASSIFICATION OF THIS PAGE (When Data Entered)

laser, rather than as an end cavity reflection of a linear laser. Various schemes and media were investigated (sodium vapor, amplifier-absorber jet, saturable absorber thin jet, saturable absorber coupled by evanescent wave). The largest nonlinear third order susceptibility was found in the amplifier jet. Study of fast dynamics of DFWM in an absorber led us to develop a ring laser producing pulses shorter than 55 fs, tunable in a 20 nm range. The measurements of DFWM inside the absorber jet of a ring laser are the basis of a new diagnostic method to measure very short ($\lesssim$ 100 fs) relaxation rates.

PHASE CONJUGATION IN A RING LASER CAVITY

J.-C. Diels

PHASE CONJUGATION IN A LASER CAVITY.

I. MOTIVATION.

We have initiated a study of the dynamics of phase conjugated coupling in a laser cavity. The research was motivated by two potential applications where intracavity phase conjugation could play an important role:

1. Prevention (compensation) of self-phase modulation, and self focussing effects in a high power laser.
2. Laser gyros.

It can easily be seen that replacement of a cavity mirror by a phase conjugated mirror will prevent self focussing in, for instance, a laser rod. This is one of the first applications for phase conjugation, and it has been proposed by numerous investigators. Instabilities can develope as fast as the beat note between two distant modes in the laser cavity. Therefore, this application requires fast tenporal phase conjugation. In this context, fast compensation implies as fast as the inverse of the gain medium bandwidth, hence picoseconds. Degenerate four wave mixing (DFWM) is one of the most commonly cited and promissing mechanism for fast and efficient phase conjugation. One of the questions answered by this research program is: can a nonlinearity be found that satisfies simultaneously the requirements of large reflection coefficients (of the order of unity) and fast (picosecond) response for phase conjugation by DFWM.

Application of phase conjugation to the operation of a laser gyro is a new application that we proposed and studied theoretically in this program.

II. DFWM IN A LASER GYRO.

The results of that theory have been summarized in a publication [1] (appendix A) and detailled in a PhD thesis [2]. There are two important findings:

1. A phase conjugated coupling introduced in the ring cavity of a laser gyro effectively reduces the "lock-in" frequency, thereby making the gyro sensitive to lower rotations speeds.
2. The DFWM coupling introduced in a ring laser cavity opposes the effect of mutual saturation which is detrimental to gyro operation. As a consequence, any laser medium, even purely homogeneously broadened, becomes a candidate for gyro operation, provided a

suitable intracavity DFWM scheme can be implemented. We believe the second property to be particularly important, since it opens the way, for instance, to the possible development of solid state integrated optics laser gyros. Subnanosecond response times are also needed for this application, if very high rotation speeds are to be measured.

III. REQUIREMENTS FOR FAST TEMPORAL PHASE CONJUGATION (theory of transient DFWM).

We have made a theoretical study of the dynamics of DFWM. In a first study published in Applied Physics [3] (Appendix B), the nonlinear interaction was considered to be extremely fast (i. e. a "steady state" nonlinear susceptibility was used). Under these ideal conditions, two fundamental limitations were established for simultaneous fast temporal and spatial phase conjugation by DFWM:

1. a thin medium (shorter than the pulse length) is required.
2. the medium has to be optically thin (the gain of the probe has to be small). This last condition implies that it is not possible to have simultaneously a large response and temporal phase conjugation.

These two conditions have lead us into a search for thin DFWM geometries (dye jets, evanescent wave coupling) compatible with intracavity use, and intense but broadband nonlinearities. The conflicting requirements for large and fast temporal responses precludes the use of sharp resonant enhancements. It also suggests that, in order to prevent or compensate effectively self phase modulation and self focussing, a 100 % reflecting DFWM mirror should not be used. Instead, weak phase conjugate coupling between counterpropagating beams of a ring laser could provide the compensation sought for, without the distortion introduced by an optically thick phase conjugator. As possible candidates for intense and fast DFWM mixing, we have made experimental and theoretical research on

- Sodium vapor (section IV)
- Saturable absorbers in waveguide dye lasers (section V);
- Dye jets in a laser cavity:
    - Gain-Absorber mixture (section VI.1)
    - Amplifier jet (section VI.2)
    - Absorber jet (section VI.4)
    - Absorber jet and evanescent wave coupling (section VI.5).

Femtosecond laser developments required for the absorptive DFWM are reported in section VI.3.

Other findings on transient Nonlinear Four-Wave Mixing.

Other results of our numerical and analytical study of transient DFWM can be summarized as follows (cfr. ref. [3] and [4]):

a) Square pulses are generated in the case where only one of the conditions above is satisfied (optically thin medium, but physically long compared with the pulse length).
b) In the case of absorptive nonlinearities, the "square pulse" remains a good solution up to media thicknesses of the order of the absorption length.
c) In the case of optically thick media, the curve of probe transmission versus pump power (or medium thickness, at constant pump power) exhibits hysteresis, which suggest that multistable operation should be possible. However, such a possibility is disprooved by our computer simulations, which show that, with increasing medium length, the transmission has a unique (and stable) solution, which becomes an oscillatory solution, to turn finally into a chaotic solution.

Transient DFWM with coherent interaction.

We have extended the study of transient DFWM to the case where the nonlinear susceptibility is due to two-photon resonant interaction, and the excitation pulses are applied in a time short or comparable with the phase relaxation time T2. The results of this study are contained in a PhD thesis [4] (pp 109-119), and the main findings are listed below.

a) The results in the short T_2 limit are the same as reported above and in ref [3] (Appendix B).
b) As T_2 is increased from very small values, the DFWM reflectivity increases to a constant and maximum value approached when T_2 reaches c/ℓ (where ℓ is the medium thickness).
c) The signal ressembles the convolution of pump and probe, except for pump intensities such that the pulse area is much larger than pi/2, where significant broadening of the signal is seen to occur.

The case of a single photon resonant interaction was also considered. In that case, the signal no longer ressembles a correlation of the pump and probe pulses, because each pulse is essentially "extended" in the medium by the phase relaxation time T_2. Consequently, a calculation of the probe energy as a function of the delay of the pump, has a risetime of the order of the pulses leading edge, and a fall time characterized by T_2 (ref. [4], page 122). An extensive theoretical and experimental analysis of coherent resonant

DFWM has been made - partially supported by a NSF grant - and is reported in the next section.

IV. COHERENT RESONANT DFWM IN SODIUM (BACKWARD WAVE ECHOES).

The experimental set up is shown in Fig. 1. Measurements of phase conjugated reflected signals in sodium vapor were performed for various relative delays. The signal measured lead to an interesting analysis of quantum beats in backward wave echoes (ref [5], included as Appendix C) which we observed for the first time.

EXPERIMENTAL SET UP

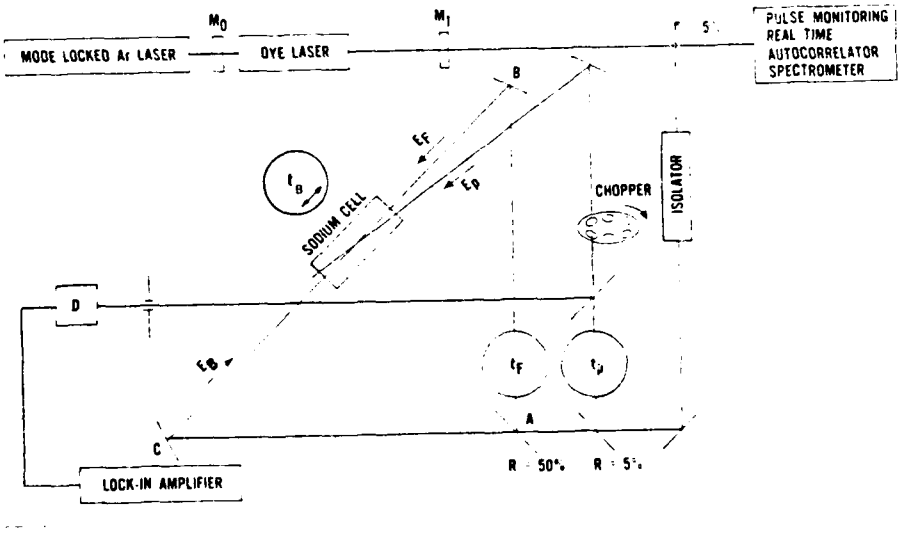

(t) OPTICAL DELAY

- ISOLATOR:
  To prevent the cavity coupling $M_0 M_1 ABCM_1 M_0$

  λ/4 Isolator:
  Inadequate (coupling through Na fluorescence)
  a FARADAY ROTATOR isolator was used

- Long Pulses (35μsec) for optimum overlap in Na cell

Figure 1.
Experimental Set-up for DFWM in Sodium Vapor.

While sodium vapor is perhaps one of the most efficient phase conjugator in the visible for CW operation, our study showed it to be unpractical in the case of an excitation by a continuous train of picosecond pulses. The problems are numerous and listed below. The most fundamental difficulties are related to the fact that the sodium linewidth, its fine structure, the mode spacing of the laser resonator (or modes of the pulse train) and of various cavities resulting from the experimental arrangement required for DFWM, are all of the same order of magnitude. The following points should be mentioned about this experiment.

1. The signal is very weak (typical reflection coefficients of 10^{-4}, and had to be discriminated against a strong fluorescence background. The signal was modulated by chopping the probe beam, and detected by a photomultiplier coupled to a lock-in amplifier.
2. Constant monitoring of the laser mode-locking is essential, because the DFWM signal, which is very small when the laser is properly mode-locked, can increase by several orders of magnitude with changes in cavity length that brings the laser out of synchronism. We have identified (by computer simulation) the appearance of "resonances" (enhancement of the signal for certain laser cavity lengths) with accidental matching of the modes of the complex cavities formed by the laser coupled to the DFWM setup, with the absorption lines (fine structure) of sodium.
3. A very small amount of resonance fluorescence (from Na) into the laser is sufficient to prevent proper mode-locked operation. A CW Faraday rotator isolator had to be used (Fig. 1).
4. A relatively complex theoretical analysis (Fig. 2) could explain the main frequency components in the observed quantum beats (the contribution of <u>all</u> the pulses of the trains - probe and pumps - had to be calculated. However, a satisfactory agreement of the signal dependence on the particular pulse sequences could not be achieved.
5. A drastic decay of the signal appeared with very small temperature increases (as little as 5 degrees C). A satisfactory modeling of this rapid decay did not appear feasible either [5].

Figure 2.
Main Steps of the Theoretical Analysis of Quantum Beats Associated with Coherent DFWM in Sodium Vapor.

THEORY (Backward Wave Echo)

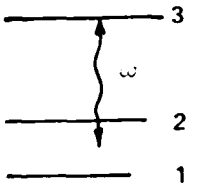

SOLVE

$$i\hbar(\partial_t + v\cdot\nabla)\rho = [H_0,\rho] + [V,\rho] - \frac{i\hbar}{2}[\Gamma,\rho]$$

$$H_0|i\rangle = \hbar\omega_i|i\rangle \qquad (i = 1,2,3,)$$

with

$$\langle i|V|j\rangle = -\tfrac{1}{2}\mu_{ij}\{E(t)e^{ikr - i\omega t} + c.c.\}$$

$$\Gamma|i\rangle = \gamma_i|i\rangle$$

specifically:

$$(\partial_t + v\cdot\nabla + \gamma_i)\rho_{ii} = a\mu_{ij}\cdot E(\rho_{ij} - \rho_{ji}) + \rho^{\circ}_{ii}$$

$$(\partial_t + v\cdot\nabla + \gamma_{ij} + i\omega_{ij})\rho_{ij} = a(\rho_{ik}\mu_{kj} - \mu_{ik}\rho_{kj})\cdot E$$

for the field sequence

$$E = E_F e^{i(k_F r - \omega t)}\delta(t - t_1) + E_p e^{i(kpr - \omega t)}\delta(t - t_2) + E_B e^{i(k_B r - \omega t)}\delta(t - t_3)$$

$$k_F - k_p + k_B = -k_p$$

$$t_2 - t_1 = t_p - t_F + mT$$

$$t_3 - t_2 = t_B - t_p + nT$$

$$t_3 - t_1 = t_B - t_F + (m + n)T$$

the signal energy is proportional to

$$\int |P(t)|^2 dt$$

where P is the velocity averaged induced dipole

$$P(t) = N\int_{-\infty}^{\infty} dv\, g(v)\,(\rho_{31}\mu_{13} + \rho_{32}\mu_{23})$$

at the "echo" time $t = t_{echo}$:

$$P = C\cdot E_F E_p^* E_B\, e^{-\frac{|v_0 k_\perp (t_3 - t_1)|^2}{4}}\left\{e^{-\gamma_3(t_3 - t_2)} + (1 - e^{-\gamma_3(t_3 - t_2)})\cos\omega_{12}(t_2 - t_1) + \cos\omega_{12}(t_3 - t_1)\right\} \times e^{-2\gamma_{31}(t_2 - t_1)}$$

The $|\sum_{n=o}^{\infty}\sum_{m=o}^{\infty}|^2$ produces terms in $\cos\omega_{12}(t_p - t_F + \psi_1)$

$\cos 2\omega_{12}(t_p - t_F + \psi_2)$

$\cos\omega_{12}(t_B - t_F + \psi_3)$

$\cos 2\omega_{12}(t_B - t_F + \psi_4)$

Conclusions

The small return signals in the above mentioned experiment, and the already excessive equipment requirements to perform these measurements, convinced us to postpone the more complex experiment of intracavity DFWM where sodium is coupled by frustrated total internal reflection to a mode-locked laser cavity (experiment planned in the original proposal). Instead, we have investigated other schemes of intracavity DFWM, using broadband saturable absorbers, as reported in the following sections.

V. SATURABLE ABSORBERS IN WAVEGUIDE DYE LASERS.

We have implemented the concept of a waveguide dye laser turning mirror suggested in the original proposal. The waveguide dye laser is confined between the reflecting face of a turning prism, and a window for the pump radiation (Fig. 3). Two counterpropagating "pump beams" for DFWM are thus confined in a planar waveguide structure of 50 μm thickness. The coupling of the forward and backward wave with the nonlinear medium (the lasing dye solution) will depend on the index of refraction of the dye solution. We choose methanol as a solvent in order to have total reflection at the interface, and coupling through the evanescent wave. Observation of a DFWM signal was hindered by the strong fluorescence background, which was difficult to eliminate because the energy source for the waveguide dye laser was also pulsed (frequency doubled Nd YAG laser). Our subsequent results with the amplifier dye jet indicate that the mutual coherence of the counterpropagating beams in the waveguide structure may not have been sufficient for DFWM to occur (this effect is discussed in more details in ref. 7, included as Appendix E).

It appears that the idea of the waveguide dye laser coupled by evanescence wave was found by some to have merit: a group in the USSR has constructed an oscillator-amplifier system based on this principle (fig 4). The analogy with the scheme suggested in the proposal is striking.

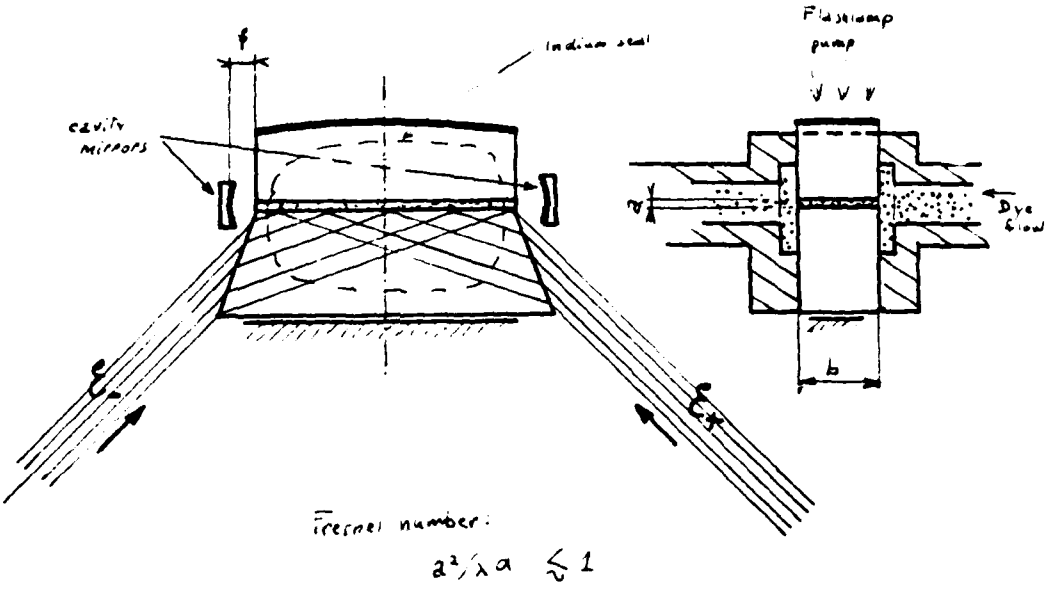

Figure 3.
Waveguide Dye Laser Turning Mirror.

Interesting schemes of quasi-planar "hollow" waveguide lasers were reported by V. M. Arutunyan, G. P. Jotyan, A. V. Karmenyan, and T. E. Meliksetyan. The "waveguide" is the active medium (a solution of Rh6G) sandwiched between two prisms. The laser light is coupled through the total internal reflection angle of the prisms (see Fig. 2). Oscillator-amplifier combinations have been demonstrated. Pumping occurs generally directly. Pumping through TIR has also been demonstrated.

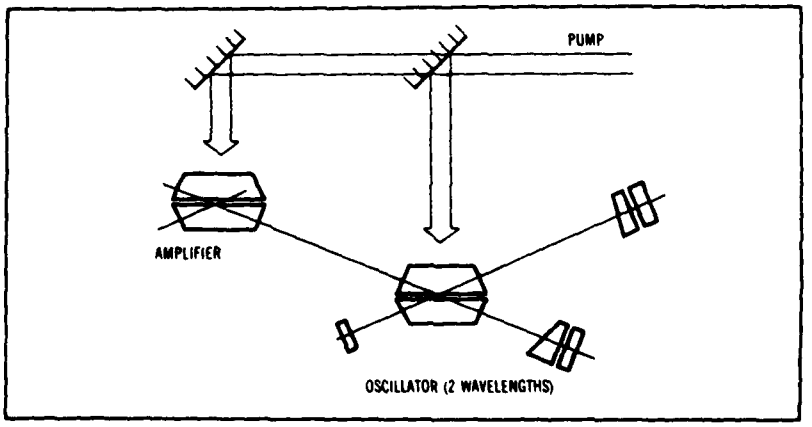

Figure 2. *Quasi-planar "hollow" waveguide laser schematic.*

Figure 4
Excerpt from "Laser Focus",
May 1983; p28.

VI. DYE JETS IN A LASER CAVITY.

Dye jets have an important advantage over any other condensed matter media and even over dye cells: they can handle much higher average powers. Another advantage is that, because of the broad bandwidth of the absorption, the response time of the nonlinear interaction is expected to be subpicosecond. In the studies described below (with the exception of section VI.1), we have used the dye jet inside a ring laser cavity, in such a geometry as to impose simultaneity of counterpropagating pulses in the dye jet.

VI.1 DFWM in the Mixed Gain-Absorber Medium of a Passively Mode-locked dye laser.

In the linear cavity sketched in Fig. 5 we observed the simplest and most dramatic evidence of the importance of DFWM in the operation of a mode-locked laser. The linear cavity is that of a passively mode-locked dye laser pumped by a continuous argon laser. A particular case of DFWM causes the output of this laser to consist of two interwoven pulse trains separated by 1/3 ns. The first pulse experiences the largest gain when passing through the dye solution from right to left (Fig. 5a). When this pulse returns to the dye jet after reflection on the end cavity mirror, it "collides" with the second one, creating a population grating in the jet (Fig. 5b). Scattering of the first pulse on this grating will result in an amplification of the second pulse (travelling to the left in Fig. 5b).

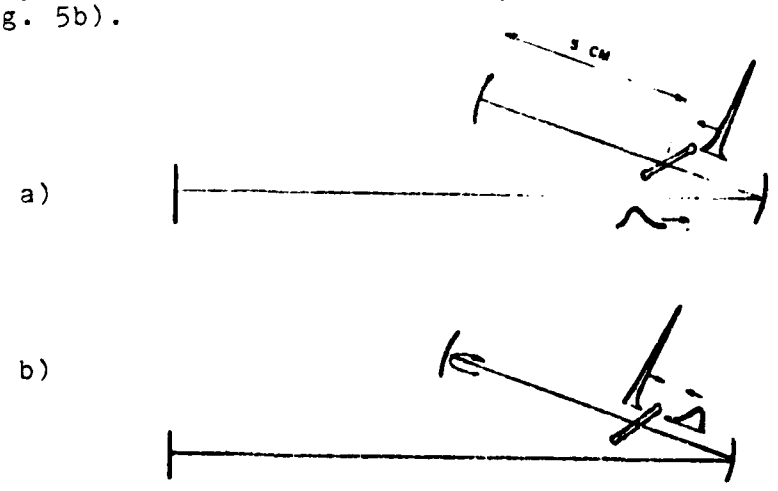

Figure 5.
Mutual Interaction of two Counterpropagating Beams in a Mode-Locked Linear Dye Laser Cavity.

The second pulse being much longer than the first one, cross correlating the first and second pulse enabled us for the first time to measure accurately a subpicosecond pulse shape, and to use it as a stringent test for theoretical modeling of the mode-locked dye laser and of the mechanism of DFWM in the dye jet. This work was reported at the XIIth International Quantum Electronics Conference in Munich [6] and at the IIIrd Int. Picosecond Conference in Garmisch Partenkirschen [7] (Appendix D). The major conclusions to draw from this section are listed below.

a) A very small intracavity DFWM effect can have a major effect on the operation of a mode-locked dye laser (even creating an additional pulse train as in the present situation).

b) A simple model based on rate equations can give an accurate description of the operation of the mode-locked dye laser and of the mutual coupling of two counterpropagating pulses in the dye jet. The agreement between theory and experiment is demonstrated in Fig. 6.

c) Our work took the finite thickness of the dye jet into account. By applying our theoretical model to the ring dye laser, we were able to demonstrate the stabilizing effet of the absorber jet, as well as the limiting influence of the absorber jet thickness on the pulse duration [7].

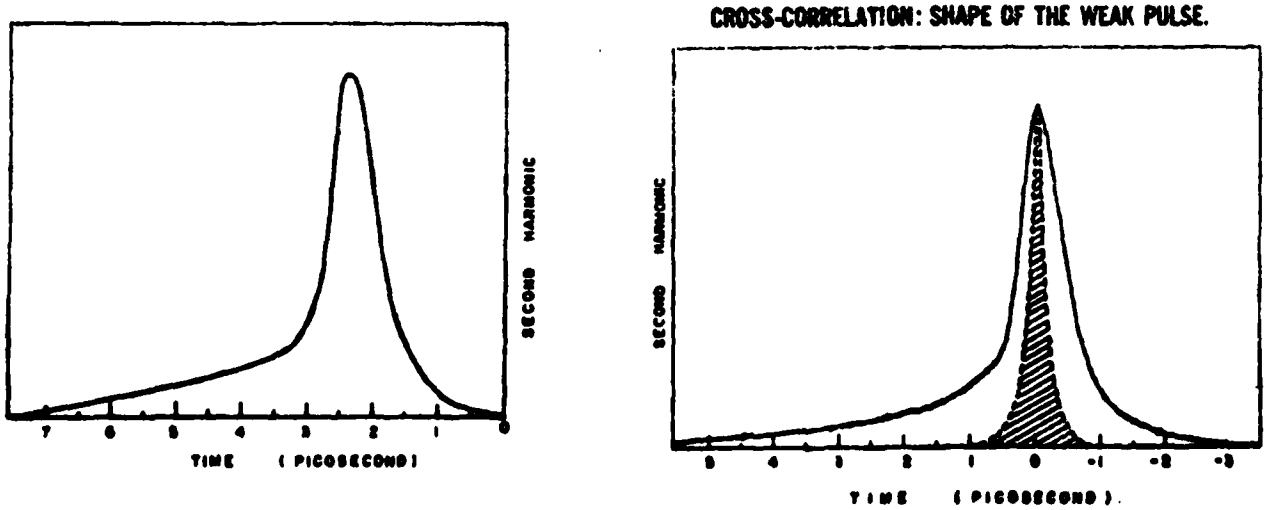

Theory Experiment

Figure 6.

VI.2 Picosecond DFWM in an Amplifier Jet of a Synchronously Mode-locked Ring Dye Laser.

In this section and in the followings, the two "strong" or "pump" beams for DFWM are provided by the counterpropagating beams in a ring laser cavity. We presented [8] the first demonstration of DFWM of picosecond pulses in a saturable amplifier. Our theoretical model, accounting for the transient nature of the interaction, provides an accurate match to the experimental data. This work has been reported in details in ref [8] (included as Appendix E). The ring laser (sketched in Fig. 7) is synchronously pumped by an argon laser operating at roughly 240 MHz. Our data show that the transient nonlinearity could be assimilated to a constant third order susceptibility (one of the largest broadband DFWM type nonlinearity in the visible) of 10^{-8} m^2/V^2 up to a DFWM reflection coefficient of 1 %. The range of probe delays over which the signal could be observed established that the mutual coherence of the counterpropagating beams in the dye laser is only 0.6 ps, which corresponds to the dye jet thickness. We ascribe this short coherence time to mutual saturation of the intracavity beams in the amplifier jet, which favors an incoherent superposition of fields at that location. Some degree of mutual coherence was forced upon the counterpropagating laser beams by the picosecond pump pulses. It was impossible to observe DFWM with continuous pumping, and simple interferometric measurements demonstrated that indeed, the absence of signal was due to mutual incoherence of the fields meeting in the jet. Our study shows also that the maximum DFWM signal is ten times larger in a saturable amplifier than in the corresponding saturable absorber. The very strong fluorescence backgroung in the case of the amplifying medium is however a disadvantage in many applications.

Figure 7
Ring Laser Cavity and
Experimental Set-up for DFWM in the Amplifier Jet.

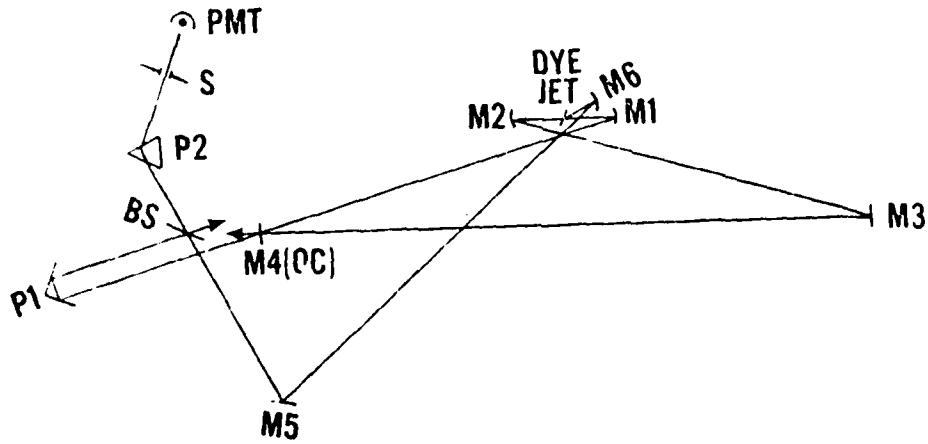

VI.3 Femtosecond pulse generation.

The ring laser reported in this section [9] (Appendix F) was needed as a source for the studies of femtosecond DFWM described in the next two sections. The two main goals were:

- to develope a stable femtosecond ring dye laser in which the two counterpropagating intracavity pulses meet exactly in the absorber jet;
- to study the influence of intracavity glass on the operation of such a laser.

This study scored a major technological record and a scientific achievement.

Technological success:

We measured autocorrelation widths of 82 fs (corresponding to pulse durations of less than 55 fs, the shortest ever produced directly by a laser) with a TUNABILITY range of 250 nm.

Scientific Achievement:

We identified the mechanism of ultrashort pulse formation with successive downchirping (decreasing frequency phase modulation) in the dye jet and pulse compression in the glass prism (by propagation of a "downchirped" pulse in a medium with normal dispersion). We believe that the same mechanism of intracavity downchirping - compression by normal dispersion - takes place in any of the ring femtosecond lasers reported to date. However, the role of the prism is replaced by that of the complex reflection coefficient of one of the laser cavity mirrors. We have observed that indeed, in all the lasers in operation, there is at least one cavity mirror that is being used near the edge of a reflective coating, where the dispersion in complex reflectivity is the largest. The normal dispersion properties of a dielectric coating were recently confirmed through computer calculations by Dr Svelto, who verified quantitatively the ability of a cavity mirror to produce the same pulse compression as in our laser [9]. It should be pointed out however, that in our laser, in contrast to all other femtosecond ring lasers, the wavelength and the amount of compression are adjustable.

VI.4 Femtosecond DFWM in an Absorber Jet of a Passively Mode-locked Ring Dye Laser.

The saturable absorber of a femtosecond ring dye laser such as the one described in the preceeding section is a nearly ideal candidate for the study of fast transient DFWM. The advantages of using the absorber dye jet inside the mode-locked laser cavity as nonlinear medium are listed below.

a) The two counterpropagating pulses in the ring laser meet exactly at the dye jet at each round-trip, The problem of "timing" the DFWM pump pulses is therefore automatically solved.
b) The energy of the pulses inside the cavity is such that the absorber dye is saturated, which is the condition required for efficient DFWM.
c) The nonlinear medium is narrow (50 m), which is a necessary condition to study fast transients in DFWM.

The probe beam is taken from one output of the dye laser, and focussed into the interaction region in the absorber jet, at 45 degrees with the pump beams, after passing through an adjustable optical delay (Fig. 8). In the experimental set up of Fig. 8, the phase conjugated signal is recorded by a photomultiplier tube, as a function of the delay of the probe. In another set up described at the end of this section, the temporal shape of the signal is inferred from a cross-correlation of the signal with the laser pulse. The measurements of DFWM signal are performed for parallel and perpendicular polarisation (of the probe with respect to the pump beams).

With these measurements, we are developping a new method of study of optical and physical properties of absorbing dyes in a yet unexplored time domain. We expect that these measurements will provide new physical data on organic dye molecules. For instance, these measurements will enable us to determine the phase relaxation time of dye solutions. This time sets a lower limit to the pulse duration that can be achieved in any laser or switch (for instance DFWM switch) of which it is a component. A particularly interesting parameter from the data presented below is the ratio of the maximum signal energy in parallel and crossed which varies strongly with pulse duration and nature of the dye. The analysis of the data is complex and not completed yet. Some typical data are presented below.

Figure 8.
Experimental set up for the observation of DFWM in the saturable absorber jet of a mode-locked ring dye laser. The laser beams inside the cavity are represented by a solid line (path M1-M2-M5-M4-M3-M6-M1). One of the outputs at M5 is sent via an optical delay (the prism P1 is mounted on a translation stage) into the absorber. The "reflected" DFWM signal is deflected by a beam splitter (BS) into the photo-multiplier (PMT).

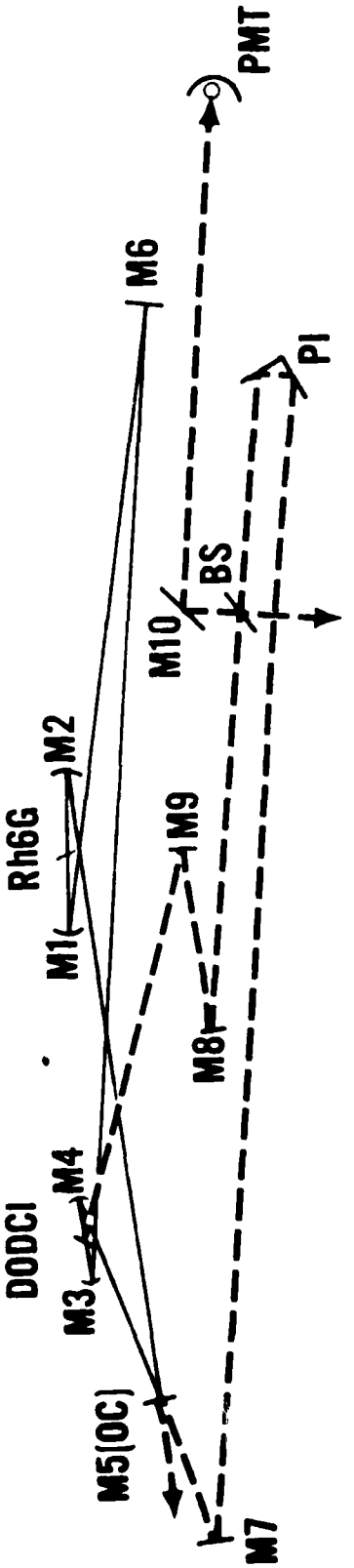

Figure 9

Comparison of the DFWM signal versus delay for DQOCI (di-ethylquinolyoxacarbocyanine iodide) and for DODCI (di-ethyloxadicarbocyanine iodide), for crossed and parallel polarisation. The laser pulse durations are indicated (97 fs for DQOCI, and 83 fs for DODCI). The signal in crossed polarisation is much larger in the case of DQOCI.

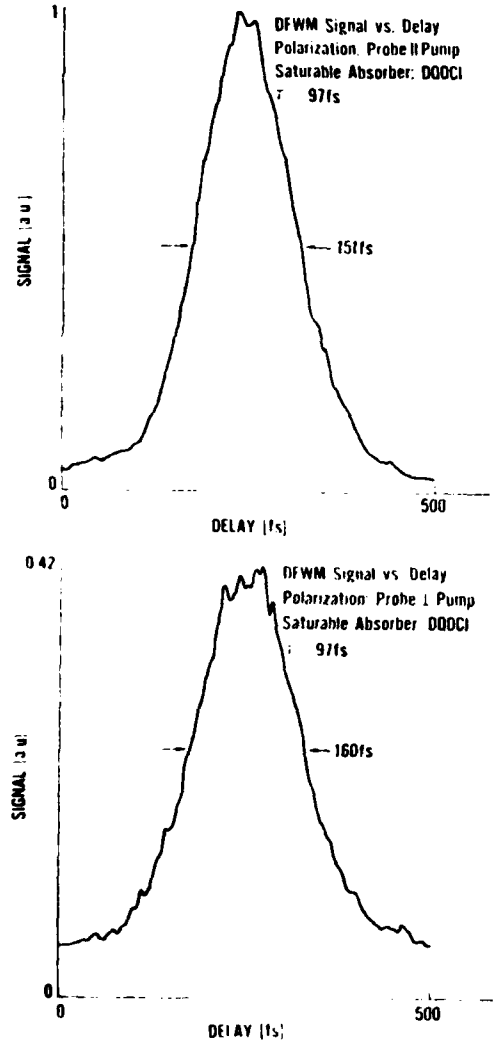

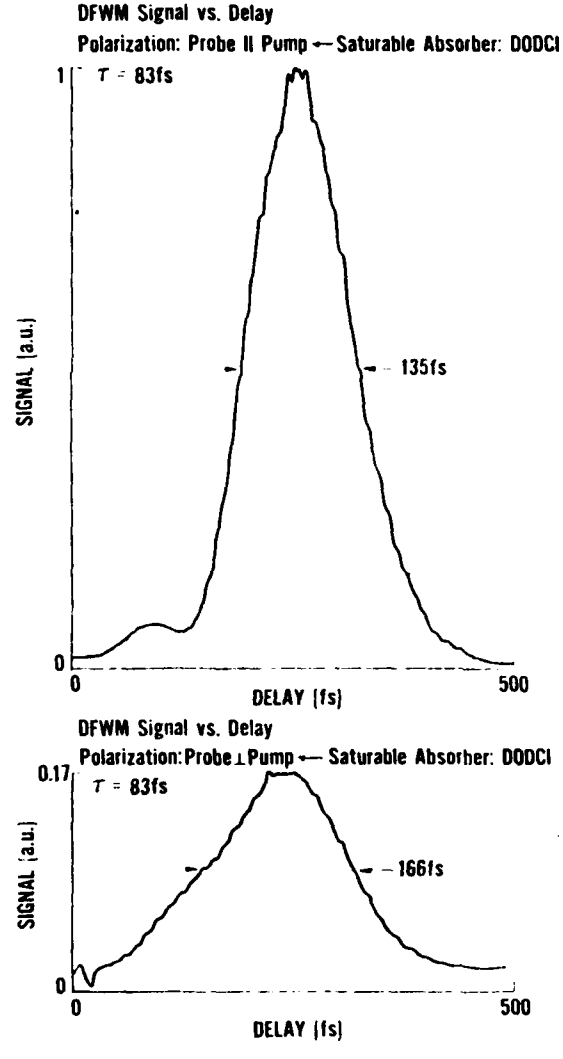

Figure 10

Comparison of the DFWM signal versus delay for long pulses (670 fs) and for short pulses (83 fs). Relatively to the pulse duration, the signal extends over a much shorter delay in the case of the long pulse. Also in the latter case, the signal in crossed polarisation is relatively much more intense.

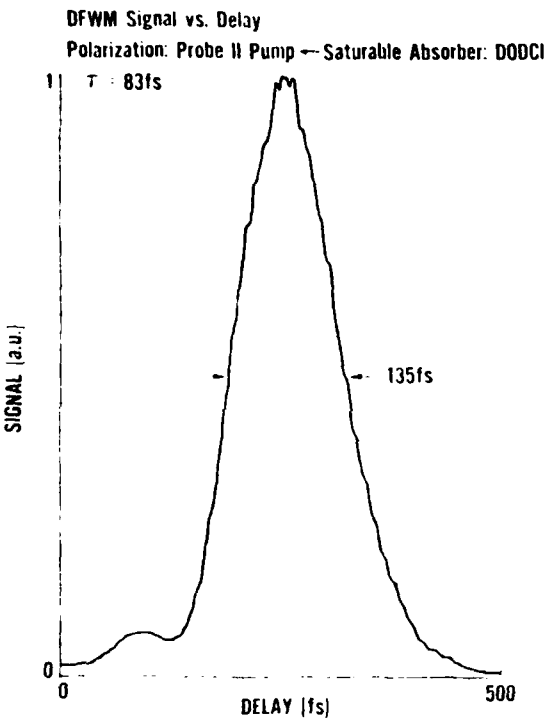

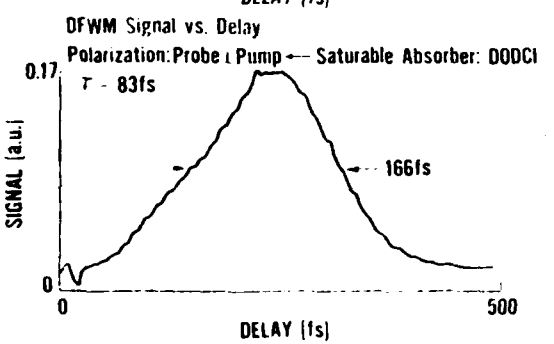

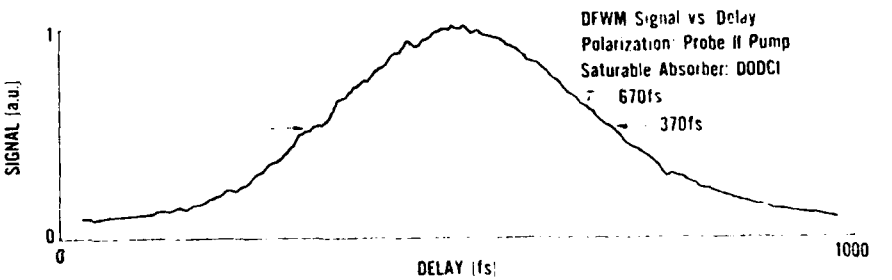

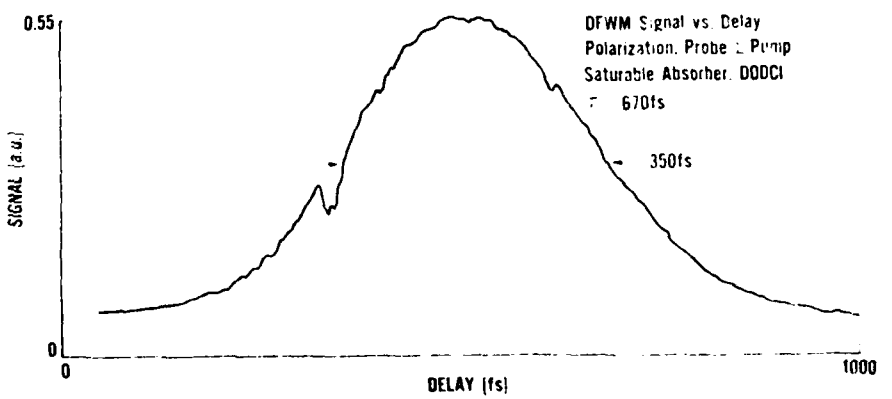

Figure 11.

Measurement of the cross-correlation of the DFWM signal with the pulse from the laser. of The return signal and the complement of the probe (at the beamsplitter BS) are sent cross polarised with respect to each other into a urea crystal. The cross correlation is the type II second harmonic signal generated in a urea crystal, as function of the position of the delay prism P2. The sensitivity of this arrangement was measured to be 10^{-6} for the laser power presently available.

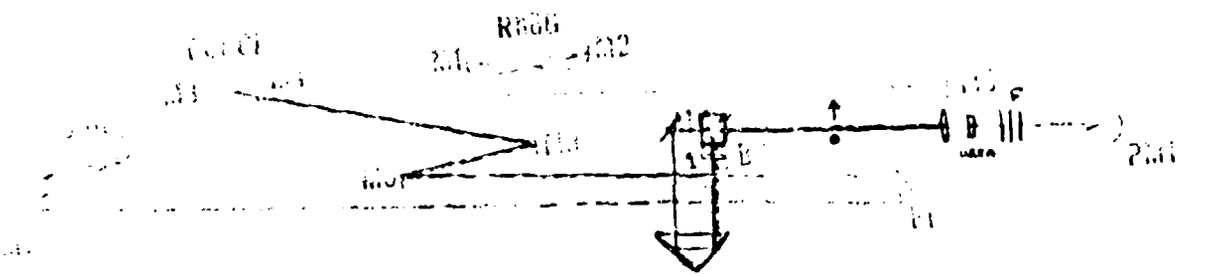

Figure 12

Recording of the cross-correlation of the DFWM signal with the laser pulse.

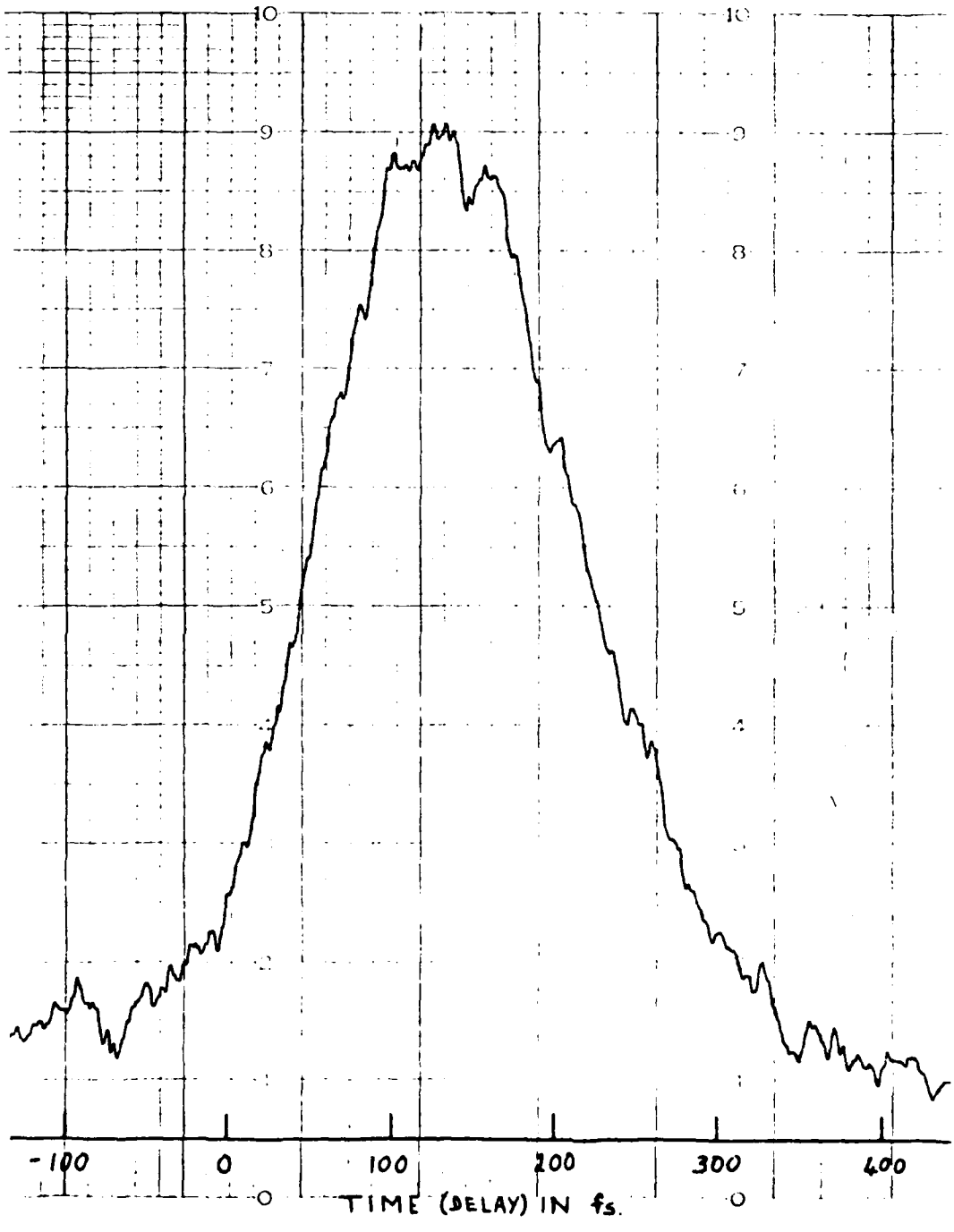

VI.5 DFWM in a Saturable Absorber "Evanescent Wave Coupled" to a Passively Mode-locked Ring Dye Laser.

Our measurements and theory (ref [6, 7] have shown that the thickness of the absorbing dye jet limits the pulse duration. In order to produce even shorter pulses, and to improve the temporal resolution of the experiments described in the preceeding section, it would be desirable to confine the saturable absorber in a shorter length. Instead of using the saturable absorber to modulate the transmission through a liquid jet, we have attempted [9] (Appendix G) to modulate the total internal reflection at a glass- dye solution interface. Unless the saturation intensity is reached in the dye solution by the evanescent wave, absorption of the latter will preclude total reflection. Tighter focussing is required than in the dye jet used in transmission, because of the fast decay of the field (Fig. 13). The penetration depth α^{-1} is given by:

$$\alpha = \frac{2}{\lambda}\sqrt{n_1^2 \sin^2\theta - n_2^2} + \alpha_{dye}$$

Efficient modulation of the reflection requires that:

$$\alpha_{dye} \gtrsim \frac{2}{\lambda}\sqrt{n_1^2 \sin^2\theta - n_2^2}$$

Numerical estimates show that, if α_s is the (saturated) absorption coefficient corresponding to the field at the surface, the absorption coefficient averaged over the evanescent region, is approximately $2\alpha_s$. Therefore, a higher intensity Io (tighter focussing) must be reached at the total reflection interface, than at the surface of a dye jet used in transmission.

Another difficulty associated with an evanescent wave saturation switch is the dye photolysis. The problem of dye degradation is circumvented by replenishing the dye fast. Unfortunately, surface tension reduces the flow velocity at the surface to zero, resulting in a total irreversible destruction of the dye in circa 30 s. By coating the glass with a monolayer of stearic acid (to increase the solid-liquid interface "contact angle") and using a viscous solvent (ethylene glycol), adequate flow velocities were obtained at the surface.

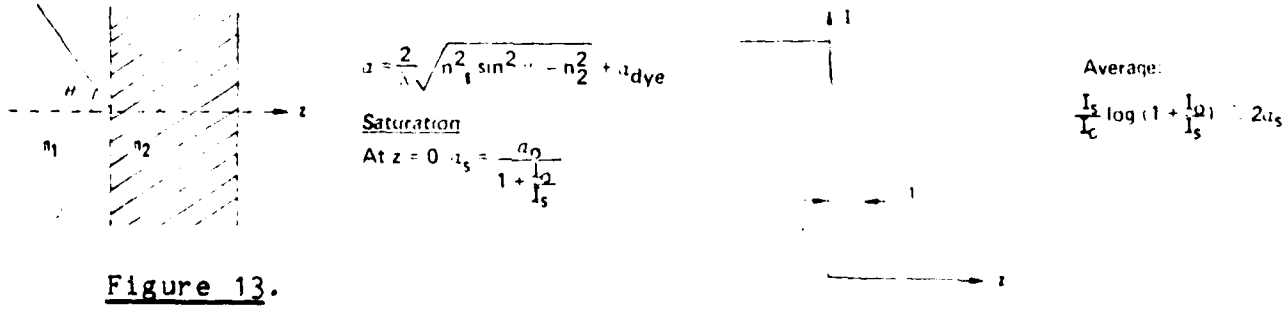

Figure 13.

The laser cavity used for the tests is sketched in Fig. 14. Incomplete mode-locking was observed. However, these attempts were made prior to the development of the successfull ring laser cavity design used in sections VI.3 and VI.4. We believe that our experience in optimizing the femtosecond ring laser cavity will enable us to implement successfully the "evanescent wave coupled mode-locker" concept.

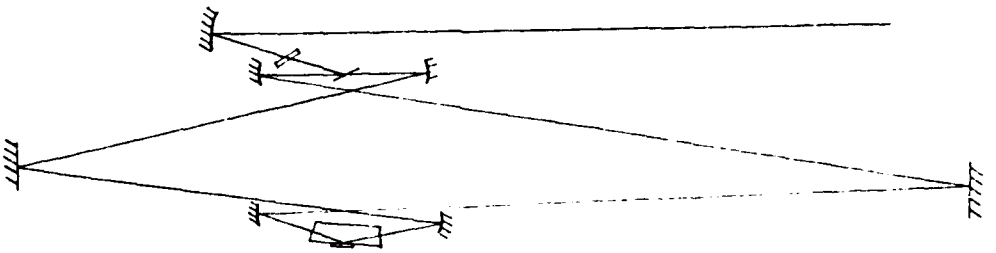

Experimental Setup

Figure 14.

The prism assemblies used for these experiments are shown in Figs 15 and 16. In the first design, the dye is flowed through a sealed cell (Fig. 15). In the second design, a free flowing jet of dye solution is squirted on the total internal reflection interface (Fig. 16).

Figure 15.

Dye Cell with the Total Internal Reflection Prism.

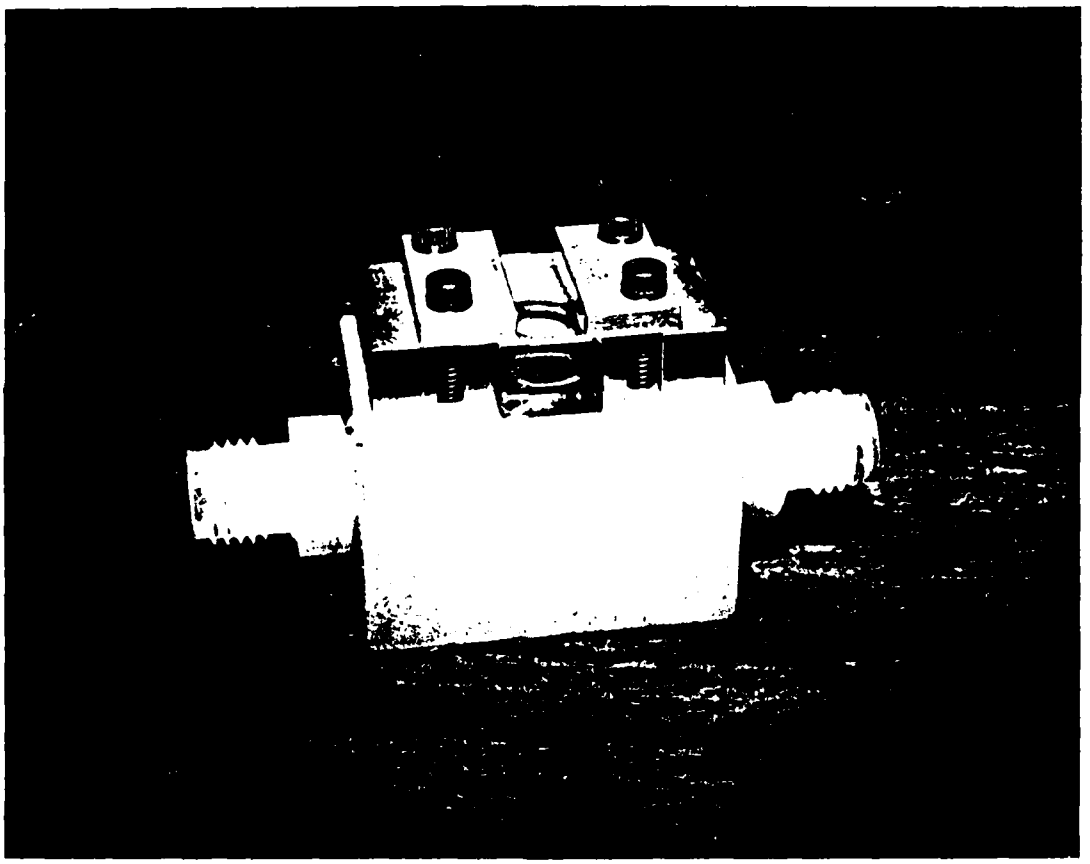

Figure 16.

Total Internal Reflection Prism Mounted on Dye Catcher Tube.

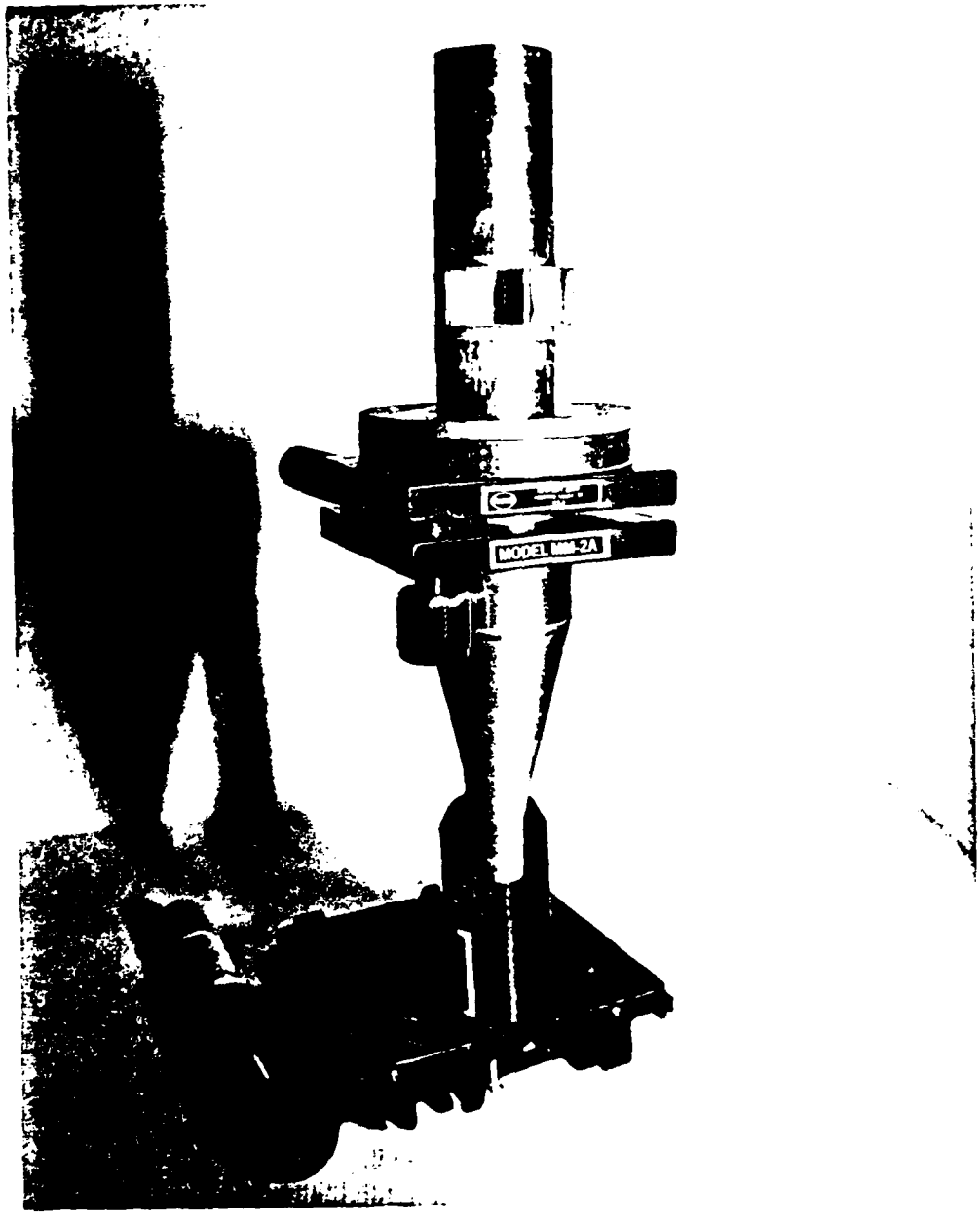

VII. EXTERNAL CIRCUMSTANCES THAT AFFECTED THE PERFORMANCES ON THIS WORK.

The project was started at the Center for Laser Studies of the University of Southern California (USC), using a provisory facility, too small to contain the equipment used in this project. Construction delays forced successive postponements of the move to a new building at USC. Unfortunately, the latter had not been designed for research in physics (inadequate temperature control and ventilation, no equipment access door, no adequate water supply). Since the administration of USC showed no intent to make these rooms functional as laboratories, and after the loss of 3 argon laser tubes, I resigned from the Center for Laser Studies to move to North Texas State University in september 1981. Thanks to a low overhead rate at NTSU, the equipment lost to USC could be replaced promptly. Nevertheless, the perturbation produced by two successive moves did introduce some delays in the research performances.

VIII. RECOMMENDATIONS FOR FUTURE WORK.

1. Femtosecond DFWM.

The measurements of femtosecond DFWM described in section VI.4 point to a new diagnostic method that should be investigated further. From the point of view of basic physics and chemistry, this new technique will contribute to the understanding of the dynamics of dye molecules in solution, by providing information on parameters hitherto inaccessible by other methods. A systematic method to investigate dynamical parameters of fast dyes for mode-locking and fast shutters (for instance by DFWM) is important for the development of femtosecond techniques.

2. Development of femtosecond lasers.

We have gained a better understanding of the operation of mode-locked dye lasers. Hybrid (passive-active) mode-locking should lead to the production of pulses of larger energy, and enable us to use a frequency-doubled Nd:YAG laser as a pump source, rather than to be at the mercy of the expensive and capricious argon laser technology.

Promissing also is the use of evanescent wave coupled saturable absorbers, which have the advantages of

a) replacing a jet of typically several tenth of microns by an equivalent absorber thickness of the order of one micron;
b) providing a stable flat optical surface as reference for the

femtosecond laser pulses, rather than the surface of the jet which is usually of poor optical quality, and moves with air currents and acoustic perturbations.

There is a need for high energy femtosecond pulses. The use of single mode fibers for pulse compression is limited to pulses of low energy, because of the small cross-section of the fibers. Two alternate methods emerge from the work reported here.

a) Compression through the amplification of pulses of controllable chirp. Since the laser reported in section VI.3 produces pulses with an adjustable down-chirp, they could be optimized for maximum compression through the normally dispersive optics of the amplifier chain.
b) Compression through coherent propagation through a resonant absorber. The ideal medium for this experiment has to be determined through measurements of the type reported in section VI.4. Dye solutions are ideal candidates, provided a suitable dye can be found that has a phase relaxation time longer than the pulse to be compressed. Metal vapors are also possible candidates.

3. Integrated Optics Laser Gyro.

The theory reported in section II shows that an integrated optics laser gyro is physically possible. However, technological progress is required in the area of integrated optics (low scattering and phase conjugation by DFWM) before this concept can be implemented.

REFERENCES.

1. J.-C. Diels and I. C. McMichael, "Wavefront Conjugation in a Laser Gyro", Optics Letters 6, 219 (1981).

2. Ian C. McMichael, Ph.D. thesis, to be completed in fall 1983.

3. J.-C. Diels, W. C. Wang and H. Winful, "Dynamics of the Nonlinear Four-Wave Mixing Interaction", Appl. Physics, B26, 105 (1981).

4. W. C. Wang, Ph. D. thesis, July 1982.

5. R. K. Jain, H. W. K. Tom, and J.-C. Diels, "Picosecond Resolution Studies of Ground State Quantum Beats and Rapid Collisional Relaxation Processes in Sodium Vapor", 3rd Int. Conf on Picosecond Phenomena, Garmisch Partenkirchen, June 1982.

6. J.-C. Diels, J. J. Fontaine, I. C. McMichael and C. Y. Wang, "Experimental and Theoretical Study of the Mutual Interaction of Subpicosecond Pulses in Absorbing and Gain Media", XII th IQEC, Munich, june 1982.

7. J.-C. Diels, I. C. McMichael, J. J. Fontaine and C. Y. Wang, "Subpicosecond Pulse shape Measurement and Modeling of a Passively Mode-locked Dye Laser Including Mutual Interaction in a Dye Jet", 3rd Int. Conf. on Picosecond Phenomena, Garmisch Partenkirchen june 1982.

8. J.-C. Diels, I. C. McMichael and H. Vanherzeele, "Picosecond Transient Phase Conjugation in Amplifying Dyes", submitted to IEEE J. of Quantum Electronics (1983).

9. W. Dietel, J. J. Fontaine, and J.-C. Diels, "Intracavity Pulse Compression with Glass: A new Method of Generating Pulses Shorter than 60 Femtoseconds", Optics Letters 8, 4 (1983).

Influence of wave-front-conjugated coupling on the operation of a laser gyro

Jean-Claude Diels and Ian C. McMichael

Center for Laser Studies, University of Southern California, University Park, Los Angeles, California 90007

Received January 5, 1981

We present a theoretical analysis of a ring laser incorporating a wave-front-conjugating coupling element between the *counterpropagating* waves. Our results demonstrate the possibility both of using a homogeneously broadened laser, such as a solid-state or dye laser, and of a substantial reduction in lock-in frequency.

If a ring laser is rotated, the cavity round-trip time becomes different for the two oppositely directed traveling waves (ODTW's). This implies that the two ODTW's have to assume different frequencies. If portions of each of the ODTW's are allowed to exit from the cavity and are mixed, a beat frequency can be detected that is proportional to the applied rotation rate. This is the ideal laser gyro. In practice, however, there is a coupling of the ODTW's because of the backscattering of one of the ODTW's into the other. At low rotation rates, this coupling causes the ODTW to assume the same frequency, and the beat frequency disappears.[1] This frequency synchronization of the ODTW is termed lock-in.

A good *ring laser for gyro* application should have not only a minimal coupling between counterpropagating waves but also a stable standing-wave mode of operation when at rest. Homogeneously broadened gain media, such as in solid-state and dye lasers, have therefore been ruled out for gyro operation.

Kühlke[2] showed, for instance, that, in the case of cw dye lasers with weak backscattering coupling, there is generally a strong imbalance between the counterpropagating amplitudes. The laser operation even alternates between the two modes when the backscattering coupling exceeds a certain threshold. Our analysis shows that insertion of a wave-front-conjugated coupling element inside a laser cavity (1) results in reduction of the lock-in threshold and (2) reduces the imbalance between the amplitudes of the ODTW's in homogeneously broadened rotating ring lasers, making them possible candidates for gyro operation.

At any point within the ring cavity, the counterpropagating fields E are described by the slowly varying amplitude ($\mathcal{E}$) and phase (ϕ) functions:

$$E_1 = \mathcal{E}_1 \exp[i(\omega_0 t + \phi_1)],$$
$$E_2 = \mathcal{E}_2 \exp[i(\omega_0 t + \phi_2)]. \quad (1)$$

The instantaneous frequencies of the two counterpropagating waves are, respectively, $\omega_0 + \phi_1$ and $\omega_0 + \phi_2$, where ω_0 is the emission frequency of the laser at rest. At each round trip, backscattering will cause a fraction r of the field E_1, phase shifted by an angle ϵ_1, to be added to the counterpropagating field E_2, and vice versa. An intracavity wave-front-conjugating element will introduce a similar coupling between the waves E_1 and E_2. We shall consider in this Letter an ideal wave-front-conjugated coupling, as provided, for instance, by degenerate four-wave mixing at ω_0, in a medium dominated by the proximity of a two-photon resonance[3,4] [nonlinear polarization: $P_{NL} = (\chi_{NL} E_F E_B) E_i^*$, where E_F and E_B are strong counterpropagating coherent (pump) beams at ω_0, E_i is the probe beam—E_1 or E_2—and P_{NL} is the polarization counterpropagating to E_i, induced by the nonlinear susceptibility χ_{NL}]. The field configuration is sketched in Fig. 1. At each round trip, the wave-front conjugation causes a field amplitude $c\mathcal{E}_1$ to be added to the counterpropagating field E_2, with a phase $-\phi_1 + \gamma$, where γ is the constant phase angle introduced by the phase-conjugated coupling. The constant phase shift incurred by each field after traversal through the conjugating element can be incorporated into the cavity perimeter. The differential equations describing the evolution of the ODTW fields are

$$\frac{\mathrm{d}}{\mathrm{d}\frac{c_0}{l}t} E_1 = \frac{\alpha_1}{2} E_1 + [re^{i\epsilon} + ce^{-i(\phi_2 - \gamma)}]E_2, \quad (2)$$

$$\frac{\mathrm{d}}{\mathrm{d}\frac{c_0}{l}t} E_2 = \frac{\alpha_2}{2} E_2 + [re^{i\epsilon} + ce^{-i(\phi_1 - \gamma)}]E_1. \quad (3)$$

The α's are the round-trip gains, r is the backscattering

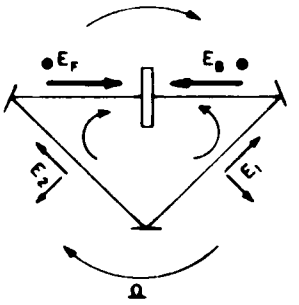

Fig. 1. Field configuration.

Reprinted from **Optics Letters**, Vol. 6, page 219, May 1981

coefficient, ϵ is the phase shift of the backscattered wave, c is the coefficient of phase-conjugated reflection, the -2ϕ's are the phase shifts of the phase-conjugated reflections, c_0 is the speed of light, and l is the length of the perimeter of the cavity. These equations can be rewritten in terms of intensities and phase of the ODTW:

$$I_1 = \frac{c_0}{l}\{\alpha_1 I_1 + 2\sqrt{I_1 I_2}\,[r\cos(\psi + \epsilon) + c\cos\varphi]\}, \quad (4)$$

$$I_2 = \frac{c_0}{l}\{\alpha_2 I_2 + 2\sqrt{I_1 I_2}\,[r\cos(\psi - \epsilon) + c\cos\varphi]\}, \quad (5)$$

$$\dot{\psi} = R\Omega - \frac{c_0}{l}\frac{1}{\sqrt{I_1 I_2}}\{r\,[I_1\sin(\psi - \epsilon) + I_2\sin(\psi + \epsilon)] + c(I_1 - I_2)\sin\varphi\}, \quad (6)$$

$$\dot{\varphi} = -\frac{c_0}{l}\frac{1}{\sqrt{I_1 I_2}}\{r[I_1\sin(\psi - \epsilon) - I_2\sin(\psi + \epsilon)] + c(I_1 + I_2)\sin\varphi\}, \quad (7)$$

where $\dot{\psi} = \dot{\phi}_2 - \dot{\phi}_1$ is the instantaneous beat frequency between the ODTW, $\varphi = (\phi_2 + \phi_1 + 2\gamma)$, Ω is the rotation rate of the ring laser, R is a geometrical-scale factor of the gyro[1], and I_1 and I_2 are the intensities of the counterpropagating beams. These equations are independent of the constant phase angle γ introduced by the phase-conjugated coupling. The net gain coefficients α_1 and α_2 are given by

$$\alpha_1 = \frac{\alpha_0}{1 + \beta I_1 + \theta I_2} - \alpha_L,$$

$$\alpha_2 = \frac{\alpha_0}{1 + \beta I_2 + \theta I_1} - \alpha_L, \quad (8)$$

where α_0 is the unsaturated gain and α_L represents the losses. In the denominators, the products βI_i and θI_i describe, respectively, the self-saturation and mutual saturation.

The gyro equations have a steady-state solution ($\dot{\psi} = 0$) for $c = 0$ and $\theta = \beta$ given by

$$\frac{\cos^2\epsilon}{\sin^2\psi} - \frac{\sin^2\epsilon}{\cos^2\psi} = \left(\frac{2rc_0/l}{R\Omega}\right)^2, \quad (9)$$

$$\frac{I_2}{I_1} = \frac{\cos(\psi - \epsilon)}{\cos(\psi + \epsilon)}. \quad (10)$$

The system of Eqs. (9) and (10) has a standing-wavelike solution ($I_2 \simeq I_1; \dot{\psi} = 0$) for small rotation rates ($R\Omega \ll rc_0/l$) and a nearly unidirectional solution ($I_2 \gg I_1; \psi \simeq \pi/2 - \epsilon$) for large rotation rates ($R\Omega \gg rc_0/l$). The existence of these stationary solutions for the entire range $\beta < \theta < 2\beta$ and their stability are demonstrated by numerical integration of the gyro equations (4)–(7). Given arbitrary initial values, the functions $I_1, I_2, \dot{\psi}$, and $\dot{\varphi}$ evolve toward steady-state solutions (9) and (10). For these solutions, there is no measurable beat frequency between the two ODTW's ($\dot{\psi} = 0$), and any laser with $\beta < \theta < 2\beta$ appears unsuitable for gyro operation. However, wave-front-conjugated coupling $c \neq 0$ restores a gyroscopic response for these lasers by affecting the existence or the stability of the stationary solutions. In the particular case of $\theta = \beta$ considered above, it can easily be seen that the assumption of steady state cannot be satisfied if $c = r$ for rotation such that $R\Omega > rc_0/l$. Computer analysis confirms the restoration of gyroscopic response through wave-front-conjugated coupling $c \geq r$ for all values of $\beta < \theta < 2\beta$. An example is illustrated in Fig. 2, pertaining to the extreme case in which $\theta = 2\beta$ with a rotation $R\Omega = 3.3rc_0/l$. This rotation rate is slightly above the lock-in threshold of the laser with $\theta = \beta$. For $c = 0$, the system of Eqs. (4)–(7) evolves toward a stationary solution with a strong imbalance between the intensities of the ODTW's. The time evolution of I_1, I_2, and $\dot{\psi}$, in the cases in which $c = r$ and $c = 20r$, is plotted in Fig. 2. For $c \neq 0$ the solutions are periodic with period $2\pi/R\Omega$. An average beat frequency between the two periodic waves $\langle\dot{\psi}\rangle$ can be measured:

$$\langle\dot{\psi}\rangle = \frac{\int\dot{\psi}\sqrt{I_1 I_2}\,dt}{\int\sqrt{I_1 I_2}\,dt}.$$

For $c = 20r$ there is no strong imbalance between the intensities of the ODTW's; the phase and amplitude modulation become closer to a sine wave, and the gyro response $\langle\dot{\psi}\rangle/R\Omega$ approaches unity.

For $c = r$ all gyros with $0.9\beta \leq \theta \leq 1.1\beta$ show nearly identical response. Therefore, in order to assess the influence of the wave-front-conjugated coupling on the gyroscopic response, we chose the saturation parameters $\beta = 1.02\theta$, and θ was adjusted for zero gain with $I_1 = I_2$. For this choice of parameters the functions I_1, I_2, and $\dot{\psi}$ evolve toward periodic solutions at large rotations, even for $c = 0$. We chose a backscattering coefficient $r = 10^{-4}$ and a cavity perimeter $l = 1$ m.

The gyroscopic response $\langle\dot{\psi}\rangle/R\theta$ is shown as a function of applied rotation $R\Omega$ in Fig. 3 in the case of a backscattering phase angle $\epsilon = 250°$. The dashed line corresponds to the standard gyro response ($c = 0$). The

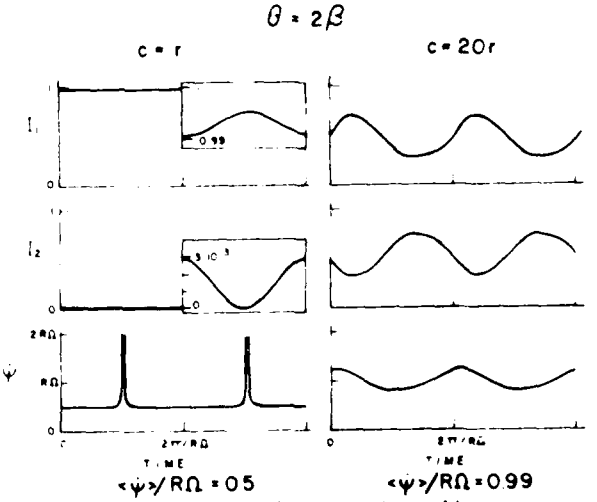

Fig. 2. Time evolution of the intensities and instantaneous beat frequency of the ODTW's in a rotating ring laser with a gain medium that is dominated by cross saturation $\theta = 2\beta$. The time evolution is shown for two values of the coefficient of phase-conjugated reflection c: $c = r$ and $c = 20r$, where r is the backscattering coefficient. In the case in which $c = r$, the scales of I_1 and I_2 have been expanded to show their periodic behavior. For this figure, the rotation $R\Omega$ is slightly above the lock-in threshold of a gyro with $\theta = \beta$. At the bottom we give the gyro response $\langle\dot{\psi}\rangle/R\Omega$ in both cases.

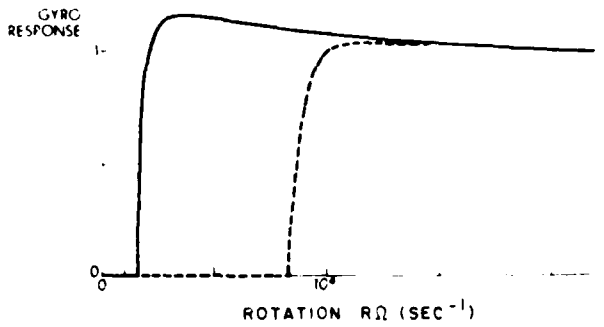

Fig. 3. Gyro response versus rotation for a rotating ring laser with a gain medium characterized by nearly equal self-saturation and cross saturation $\beta = 1.02\theta$. The gyro response is the average beat frequency between the ODTW's divided by the rotation $R\Omega$, where R is the scale factor of the gyro and Ω is the rotation rate of the gyro. The dashed line shows the gyro response in the absence of phase-conjugated coupling. The solid line is for the same gyro with the addition of phase-conjugated coupling $\epsilon = r$. For this figure, the backscattering coefficient $r = 10^{-4}$ and the cavity perimeter $l = 1$ m.

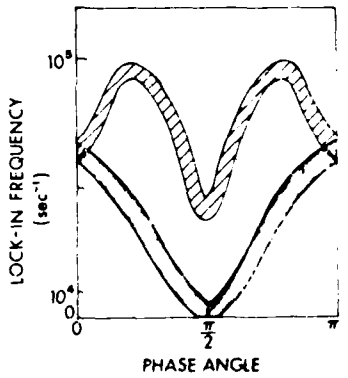

Fig. 4. Lock-in frequency versus backscattering phase angle for a gyro with nearly equal self-saturation and cross saturation $\beta = 1.02\theta$. The hatched band is for the gyro with no phase-conjugated coupling. The solid band is for a gyro with a phase-conjugated coupling $\epsilon = r$. The width of the bands indicates the boundaries within which the average beat frequency between the ODTW's vanishes. For this figure, $2r\omega_0 l = 6 \times 10^4$ sec^{-1}.

solid line corresponds to the same conditions with an additional phase-conjugated coupling of only $\epsilon = 10^{-4}$. Since the system of Eqs. (4)–(7) remains unchanged under the replacement $\psi, \Omega \rightarrow -\psi, -\Omega$, the gyro response is symmetric and is plotted only for positive rotation in Fig. 3. The lock-in frequency is seen to be substantially reduced. The reduced lock-in frequency and enhanced gyro response should be expected because the phase shifts introduced by the wave-front conjugation are *cumulative* with the ones that are due to rotation.

The backscattering (r,ϵ) that accounts for lock-in of the laser gyro is the sum of all resonant (gain medium) and nonresonant (mirrors, particles) contributions. Having showed that wave-front conjugation makes gyro operation possible for any class of laser (including waveguide), one can expect to encounter any value for the phase angle ϵ. Figure 4 illustrates the sensitivity of gyroscopic response to the backscattering phase angle ϵ. The hatched band corresponds to the case in which $\epsilon = 0$, and the solid band corresponds to the case in which $\epsilon = r$. The width of these bands corresponds to the accuracy of the calculations. The average beat frequency goes to zero somewhere within the band. Although Eqs. (9) and (10) are developed for $\beta = \theta$, they give some insight into the case in which $\beta \neq \theta$. The minima at $\epsilon = \pi/2$ correspond to the lack of a steady-state solution to Eqs. (9) and (10) for $\epsilon = \pi/2$. The bands meet at $\epsilon = 0$, consistent with the fact that Eqs. (4) and (5) are identical at $\epsilon = 0$. From Eq. (9), the lock-in rotation rate at $\epsilon = 0$ is $R\Omega = 6 \times 10^4$ sec^{-1} for the parameters chosen previously.

We conclude that, with the addition of phase-conjugated coupling, ring lasers with homogeneously broadened gain media, even when dominated by cross saturation ($\theta \gtrsim \beta$), will operate as laser gyros. In addition, phase-conjugated coupling between ODTW's in a laser gyro results in a reduction of the lock-in threshold.

This work was supported by the U.S. Office of Naval Research.

References

1. F. Aronowitz, "The laser gyro," in *Laser Applications*, M. Ross, ed. (Academic, New York, 1971), pp. 133–200.
2. D. Kuhlke and R. Herrak, Opt. Quantum Electron. **11**, 485 (1979).
3. R. L. Abrams and R. C. Lind, Opt. Lett. **2**, 95 (1978); A. Yariv, IEEE J. Quantum Electron. **QE-5**, 650 (1978).
4. J. C. Diels and W. C. Wang, to be published.

APPENDIX B

Appl. Phys. B26, 105–110 (1981)

Applied Physics

Dynamics of the Nonlinear Four-Wave Mixing Interaction

J.-C. Diels* and W.-C. Wang

Center for Laser Studies, University of Southern California, University Park, Los Angeles, CA 90007, USA

H. Winful

Advance Technology Laboratory, GTE Laboratories, Inc., 40 Sylvan Road, Waltham, MA 02154, USA

Received 23 March 1981 Accepted 25 May 1981

Abstract. We present an analysis of the impulse response of four-wave mixing, in the case where the "two-photon term" of the nonlinear susceptibility is dominant. The nonlinear interaction itself will be considered to be steady state. The conditions of negligible pump depletion are considered first. It is shown that the reflected beam has only the character of perfect phase conjugation if the pulse length is longer than the medium length, and the latter is short compared to the characteristic distance of the problem. The "weak-pulse" approximation involving only two coupled equations is compared to the exact four-wave solution, when the medium thickness approaches the critical oscillation threshold. Finally, the stability and existence of steady-state solutions is analyzed for very long media (compared with the oscillation length).

PACS: 42.65

Several effects occuring in degenerate four-wave mixing in transparent media have been predicted [1–4] and observed [5–8]. Abrams and Lind [2] demonstrated resonant enhancement of four-wave mixing through a single-photon resonance. Marburger and Lam analyzed four-wave mixing in dispersive nonlinear media, taking full account of pump depletion and intensity-dependent phase shifts. A steady-state approach was used in most work. Recently, Rigrod et al. [9], Bobroff and Haus [10], and Zel'dovich et al. [11] have considered the impulse response of degenerate four-wave mixing without pump depletion and neglecting the Kerr effect terms. The purpose of this letter is to show how the reflected beam E_B responds to a transient excitation E_F, and in the case of intense pump, whether evolution towards one or more steady-state solution(s) can be observed. The latter question is important in relation to the potential application of four-wave mixing in multistable devices [12]. The dynamics of temporal phase conjugation are important for intracavity applications of four-wave mixing [13, 14].

While the time dependence of the fields is taken completely into account, the nonlinear interaction itself will be considered to be steady state. The more complex case of transient degenerate four-wave mixing involving transient coherent nonlinear interaction will be considered in a subsequent paper. As in one of the first papers on the subject [1], we consider here the simplest case of colinear mixing of two strong counter-propagating pump waves, a forward incident probe beam of amplitude E_F, and the reflected beam E_B.

1. Propagation Equations

In an isotropic medium, the nonlinear polarization induced by an electromagnetic field **E** has two contri-

* Present address: Dept. of Physics, North Texas State University, Denton, TX 76203, USA

0340-3793/81/0026/0105/$01.20

butions, respectively, proportional to $(\mathbf{E}\cdot\mathbf{E}^*)\cdot\mathbf{E}$ and to $(\mathbf{E}\cdot\mathbf{E})\mathbf{E}^*$. The latter contribution is typical of a two-photon resonant interaction, and is responsible for wavefront conjugation in the case of colinear interaction with crossed polarization [3] (probe polarized perpendicularly to the pump fields). Only that term in the nonlinear susceptibility will be considered here:

$$P=\chi(\mathbf{E}\cdot\mathbf{E})\mathbf{E}^*. \tag{1}$$

The field E is composed of two counterpropagating "pump" beams E_1 and E_2, and a "signal" beam E_B counterpropagating to a "probe" beam E_F. In the slowly varying envelope approximation, the equation for colinear four wave mixing along the direction X are given by

$$\frac{\partial E_F}{\partial t}+c\frac{\partial E_F}{\partial X}=\frac{i\omega\chi}{4\varepsilon_0}[2E_1E_2E_B^*+(|E_F|^2+2|E_B|^2)E_F] \tag{2}$$

$$\frac{\partial E_B}{\partial t}-c\frac{\partial E_B}{\partial X}=\frac{i\omega\chi}{4\varepsilon_0}[2E_1E_2E_F^*+(|E_B|^2+2|E_F|^2)E_B] \tag{3}$$

$$\frac{\partial E_1}{\partial t}+c\frac{\partial E_1}{\partial X}=\frac{i\omega\chi}{4\varepsilon_0}[(|E_1|^2+2|E_2|^2)E_1+2E_FE_BE_2^*] \tag{4}$$

$$\frac{\partial E_2}{\partial t}-c\frac{\partial E_2}{\partial X}=\frac{i\omega\chi}{4\varepsilon_0}[(|E_2|^2+2|E_1|^2)E_2+2E_FE_BE_1^*]. \tag{5}$$

We will generally consider the situation where pump fields of constant amplitude E_{10} (for the forward propagating pump E_1) and E_{20} (for the backward propagating pump E_2), and a forward probe pulse of peak field amplitude E_0 are sent into the medium. The fields can be used to normalize (2)–(5). The pump field amplitudes E_{10} and E_{20} determine the characteristic distance

$$L_0=\left|\frac{2\varepsilon_0 c}{i\omega\chi E_{10}E_{20}}\right|. \tag{6}$$

The respective importance of pump to probe is most conveniently expressed by the use of a parameter $R=E_0^2/E_{10}E_{20}$. The phase angle ψ of the nonlinear susceptibility is defined by $\exp(i\psi)=i\chi/|\chi|$. Equations (2)–(5) are rewritten below in normalized distance ($z=X/L_0$) and time ($t'=ct/L_0$):

$$\frac{\partial\mathcal{E}_F}{\partial t'}+\frac{\partial\mathcal{E}_F}{\partial z}=e^{i\psi}\left[\mathcal{E}_1\mathcal{E}_2\mathcal{E}_B^*+\frac{R}{2}(|\mathcal{E}_F|^2+2|\mathcal{E}_B|^2)\mathcal{E}_F\right] \tag{7}$$

$$\frac{\partial\mathcal{E}_B}{\partial t'}-\frac{\partial\mathcal{E}_B}{\partial z}=e^{i\psi}\left[\mathcal{E}_1\mathcal{E}_2\mathcal{E}_F^*+\frac{R}{2}(|\mathcal{E}_B|^2+2|\mathcal{E}_F|^2)\mathcal{E}_B\right] \tag{8}$$

$$\frac{\partial\mathcal{E}_1}{\partial t'}+\frac{\partial\mathcal{E}_1}{\partial z}=e^{i\psi}\left[R\mathcal{E}_F\mathcal{E}_B\mathcal{E}_2^*+\frac{1}{2}(|\mathcal{E}_1|^2+2|\mathcal{E}_2|^2)\mathcal{E}_1\right] \tag{9}$$

$$\frac{\partial\mathcal{E}_2}{\partial t'}-\frac{\partial\mathcal{E}_2}{\partial z}=e^{i\psi}\left[R\mathcal{E}_F\mathcal{E}_B\mathcal{E}_1^*+\frac{1}{2}(|\mathcal{E}_2|^2+2|\mathcal{E}_1|^2)\mathcal{E}_2\right] \tag{10}$$

$\mathcal{E}_F$, $\mathcal{E}_B$, $\mathcal{E}_1$, and $\mathcal{E}_2$ are the normalized electric field amplitudes [$\mathcal{E}_F(z,t')=E_F(z,t')/E_0$; $\mathcal{E}_B=E_B/E_0$; $\mathcal{E}_1=E_1/E_{10}$; $\mathcal{E}_2=E_2/E_{20}$].

2. Weak-Signal Limit

In the following we will consider the medium to be irradiated by two equal counterpropagating pump fields of constant intensity at the medium boundaries $z=0$ and $z=l$. If the probe and signal are small compared with the pump fields, $R\to 0$, and pump depletion can be neglected, then the system of four coupled equations (7)–(10) reduces to two coupled equations in $\mathcal{E}_F$ and $\mathcal{E}_B$ [Eqs. (7), (8) with $R=0$ and $\mathcal{E}_1\mathcal{E}_2=1$ from Eqs. (9), (10)]. The pump depletion can be neglected if the medium is short ($l\ll 1$), or even for $l\gtrsim 1$ if the phase ψ of the interaction is such that $\cos\psi\simeq 0$. The pump fields have then constant amplitude E_0 and a nonlinear contribution to their wave vector due to the second terms in (9), (10) [$E_1=E_0\exp(\frac{3}{2}iz)$ and $E_2=E_0\exp(-\frac{3}{2}iz)$]. It is interesting to note that the solution of the constant pump approximation is independent of the phase angle ψ. In the weak probe no depletion approximation, the four-wave mixing problem yields exactly the same solution whether the nonlinear susceptibility is real or imaginary. The evolution with time of the envelopes $\mathcal{E}_F(z)\mathcal{E}_B(z)$ is independent of the phase angle ψ. As the forward propagating pulse sweeps through the nonlinear medium, it is amplified and generates the backward propagating signal. At any time, the same energy gain is experienced by each signal and given by

$$\frac{dW_F}{dt}=\frac{dW_B}{dt}=2\int_0^l|\mathcal{E}_B||\mathcal{E}_F|dz, \tag{11}$$

where the energies W_i are defined as $\int|\mathcal{E}_i|^2dz$.

The parameters of physical importance for this problem are 1) the thickness of the medium ($l\ll 1$ or $l\simeq 1$) and 2) the initial pulse shape (duration τ short or long compared with the medium; and phase modulation). The simplest situation is that of a "long pulse" sent through a "short medium". The initial pulse is amplified linearly, and the reflected pulse is the wavefront conjugated image of the initial pulse. In the approximation $l\ll 1$ and $\tau\gg l$, after passing through the medium, the field amplitudes are given by

$$\begin{aligned}&\mathcal{E}_B(\tau\to\infty, z-\tau)=e^{i\psi}\mathcal{E}_F^*(\tau=0,z)l\\&\mathcal{E}_F(\tau\to\infty, z+\tau)=\mathcal{E}_F(\tau=0,z)(1+l^2/2).\end{aligned} \tag{12}$$

The fractional energy gain of the probe $dW_F/(W_F dz)$ is simply l^2.

"Square" reflected pulses are produced when the initial pulse $\mathcal{E}_F(t=0)$ is shorter than the medium thickness

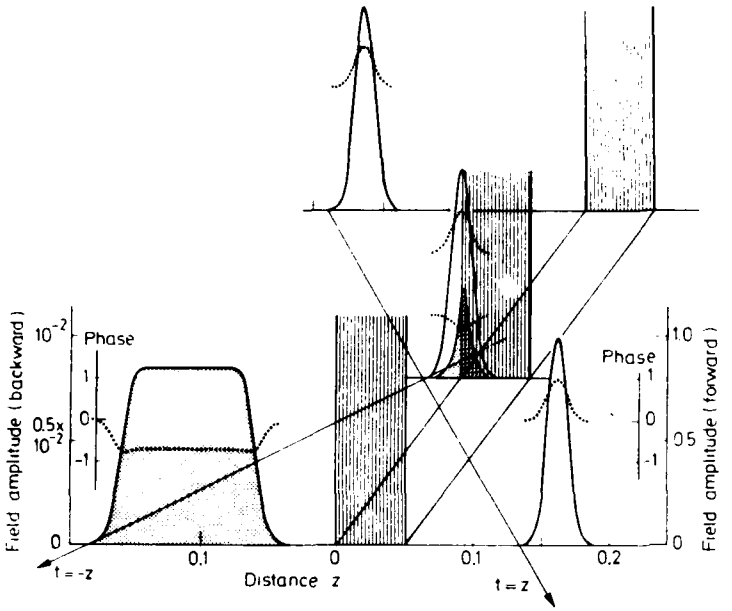

Fig. 1. Evolution with time and distance of the forward and backward field envelope. The amplitude (solid lines) and phase (dotted lines) are plotted as a function of position for three different times. The medium (thickness 0.05) is indicated by a vertical hatching. The initial pulse has a Gaussian envelope and phase modulation:

$\mathcal{E}_F(t=0,z)=\exp[-(z/0.01)^2+i\varphi_0(z)]$ with $\varphi_0(z)=\exp[-(z/0.01)^2]$

(thin medium). A maximum converted intensity is reached when the peak of the forward propagating pulse has entered the medium. The same peak intensity is constantly regenerated (Fig. 1) as the forward pulse propagates in the medium, while the same constant peak intensity is propagated backwards. It is interesting to note that temporal phase conjugation occurs only in the rise and fall of the reflected pulse. Any increase in the length of the medium (in the limit $l \ll 1$) results in a double increase of the flat portion of the square pulse without any change in peak value. More generally Marburger showed [15] that the return is proportional to the integral of the probe pulse over a round-trip time of the probe.

As the thickness of the medium becomes larger (i.e. no longer small compared to one), the conjugated signal will act itself as a source, adding a tail to the forward signal (which in turn generates a tail to the backward wave) as can be seen in Fig. 2a. These "tails" can be approximated by exponentials with the same decay constant for the forward and backward signals. These decay constants decrease with the medium thickness as shown in Fig. 2b.

A maximum converted intensity is followed by the long exponential tail mentioned above, after passage of the forward pulse through the medium. Zel'dovich et al. [11] calculated that the decay constant close to the oscillation condition ($l=\pi/2$) could be approximated by $\pi(\pi/2-l)/2l$. The Zel'dovich approximation [11] (Fig. 2b, dotted line) is seen to apply for $l \gtrsim 1$. The longest decay observed with a medium close to the critical length is similar to the "impulse response" of Rierod et al. [9] and Bobroff and Haus [10]. This is to be expected, since all memory of the initial pulse shape (in amplitude and phase) gets lost as the medium thickness approaches one. As the thickness of the medium becomes comparable to the critical oscillation length [1] $l=\pi/2$, the "weak probe" approximation will no longer be valid, when $R|\mathcal{E}_F|^2$ approaches unity. However, an exact calculation, including all terms of (7)–(10), shows that the effect of incorporating all four coupled equations is negligible for $l=1$, if $\psi=\pi/2$. If on the other hand the nonlinear susceptibility is imaginary ($\psi=\pi$ – as in the case of a two photon resonance), the two equation approximation [(7),(8) with $R\to 0$] is no longer valid. Indeed, two photon absorption will deplete the pump signals, and the product $\mathcal{E}_1\mathcal{E}_2$ will no longer be constant, but a solution of

$$\frac{\partial(\mathcal{E}_1\mathcal{E}_2)}{\partial z}=\mathcal{E}_1\mathcal{E}_2(\mathcal{E}_1^2-\mathcal{E}_2^2)/2$$

with

$$(\mathcal{E}_1\mathcal{E}_2)\,|\,\mathcal{E}_1^2+\mathcal{E}_2^2=\text{constant}.$$

In the case of $R=0.5$, the transmission and reflection of a short pulse are compared for the cases of dispersive

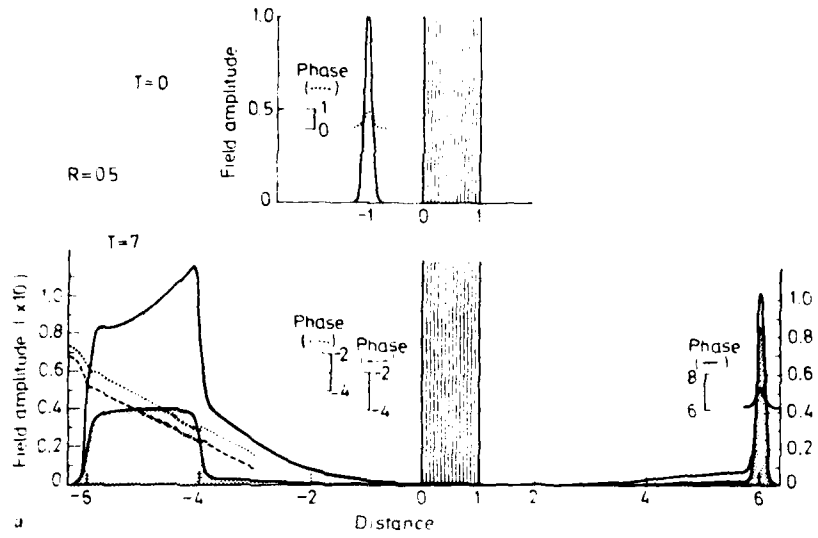

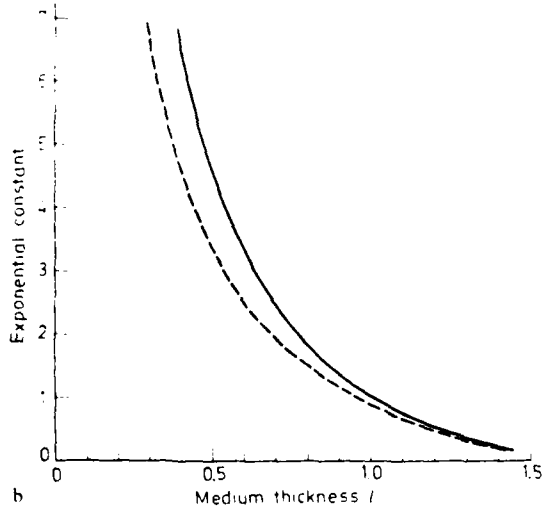

Fig. 2. (a) Propagation of a short chirped Gaussian pulse (same phase and envelope function as in the previous figure) through a four-wave mixing medium of thickness 1. The solid and dotted lines at $t = 7$ show, respectively, the spatial distribution of the amplitude and phase functions, for the reflected (left) and transmitted pulse, for the negligible depletion approximation (two equations). The exact solution (taking the four equations into account) for an absorptive nonlinearity ($\psi = \pi$) is given by the solid lines contouring the shaded areas. (b) Exponential decay constant α of the signal tail in Fig. 2 versus medium thickness l. The tail of the forward and backward propagating pulses in Fig. 2 is approximated by $\exp(\pm \alpha z)$. The distance z and thickness l are in the reduced units described in the text. The dotted line is the solution of Zel'dovich et al. [11]

($\psi = \pi/2$) or absorptive ($\psi = \pi$) nonlinear susceptibility in Fig. 2a. The lossless interaction provides a large energy transmission (1.154) and substantial reflection (0.155). The two equation approximation ($R \simeq 0$) matches perfectly the larger reflected and transmitted pulse shapes (dispersive interaction). In the case of absorptive interaction, losses prevent the exponential growth of the "reflected" signal resulting in a nearly perfect "square pulse" (shaded area). The absorption losses appear to compensate the gain responsible for the signal distortion. Figure 2a shows that, for resonant (non-dispersive) interaction, it is possible to have altogether an intense return (a large reflected energy coefficient) and square pulse generation. Two-photon resonant four-wave mixing could be used to generate square picosecond pulses of adjustable duration. The duration of the generated pulses is the sum of the probe pulse duration and the round-trip time through the interaction medium.

3. Strong-Wave Interaction

We consider now the case of a thick medium ($l > 1$) where all fields may acquire the same intensity. Equations (7)–(10) were solved numerically using a predictor-corrector method. We shall assume in the following that $R = 1$. Unlike the "weak-probe" approximation, the solution now depends on the nature of the interaction, or on the angle ψ. In the case $\psi = \pi/2$ (dispersive interaction), there is no energy left in the medium, and the following energy conservation equation must be satisfied

$$\frac{d}{dt}(W_F + W_B + W_1 + W_2)$$
$$= (|\mathcal{E}_F|^2 + |\mathcal{E}_1|^2 - |\mathcal{E}_B|^2 - |\mathcal{E}_2|^2)_{z=0}$$
$$+ (|\mathcal{E}_B|^2 + |\mathcal{E}_2|^2 - |\mathcal{E}_F|^2 - |\mathcal{E}_1|^2)_{z=0}.$$

The left-hand side is the energy lost by the fields within the medium, while the right-hand side is the flux entering the medium at the time dt.

As previously, we shall consider the case of a medium irradiated simultaneously by two constant counterpropagating pump beams. For a medium with $\Gamma = 1$, it is not clear a priori whether the transmission and reflection of a continuous probe beam will be a single-valued constant, or a multi-valued constant, or a periodic function. Two approaches can be used to study the field distributions inside the medium, and the absorption reflection coefficients.

1. A stationary approach — solving self consistently the system of (7)–(10) with the assumption that the time derivatives $\dot{\mathcal{E}}_i$ are zero;

2. Solve the system of (7)–(10) for a step function input $\mathcal{E}_F(t)$.

The first approach leads to a multivalued transmission (and reflection) for large values of the pump [12] (or for a large thickness of nonlinear material). The second approach is to let the fields inside the medium evolve with time according to the system of [7–10]. The derivation of the stationary approach is detailed first. In steady state, one can convert (7)–(10) to a set of five real equations for the amplitudes $\mathcal{E}_i (i = 1, 2, F, B)$ and relative phase θ ($\theta = \phi_1 + \phi_2 - \phi_F - \phi_B$) of the interacting waves. The amplitude equations are easily integrated to yield three conserved quantities analogous to the Manley-Rowe relations of parametric amplifier theory. These conserved quantities are

$$|\mathcal{E}_1|^2 + |\mathcal{E}_F|^2 = C_1$$

$$|\mathcal{E}_F|^2 - |\mathcal{E}_2|^2 = C_2$$

$$|\mathcal{E}_F|^2 + |\mathcal{E}_B|^2 = C_3 ,$$

where C_1, C_2, C_3 are constants which can be evaluated at the boundaries of the medium. An integration of the phase equation results in another constant

$$\Gamma = \mathcal{E}_1 \mathcal{E}_2 \mathcal{E}_F \mathcal{E}_B \cos\theta + (C_1 + C_2 + C_3)|\mathcal{E}_F|^2 - 2|\mathcal{E}_F|^4 .$$

These constants are then used to reduce the set of five equations to a single quadrature involving one variable $|\mathcal{E}_F|$, with the boundary values of the fields as parameters. The result is

$$\int_{|\mathcal{E}_F(0)|^2}^{|\mathcal{E}_F(l)|^2} \frac{d\gamma}{\sqrt{Q(\gamma, |\mathcal{E}_F(0)|^2, |\mathcal{E}_F(l)|^2, E_{10}^2)}} = l\,\Gamma_0 , \qquad (13)$$

where

$$\gamma = |\mathcal{E}_F|^2$$

and

$$Q(\gamma) = (|\mathcal{E}_F(l)|^2 - \gamma)\{[1 + |\mathcal{E}_F(0)|^2 - \gamma] \cdot [\gamma - |\mathcal{E}_F(l)|^2 + 1]\gamma - [2\gamma - |\mathcal{E}_F(0)|^2]\Gamma^2\} .$$

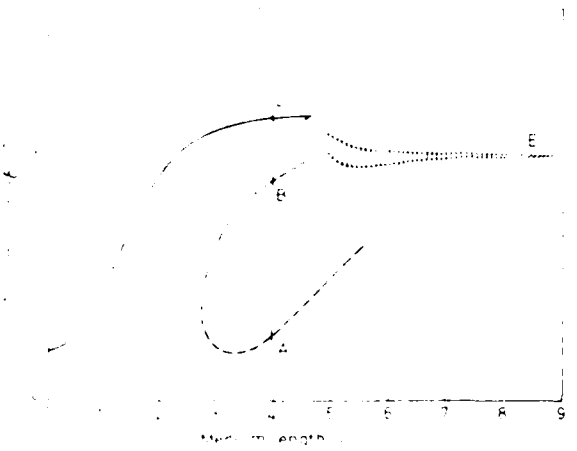

Fig. 3. Transmitted probe intensity $|\mathcal{E}_F|^2$ as a function of the medium length l. The two pump beams have equal (unit) intensity. The intensity of the forward beam sent to the medium is $|\mathcal{E}_F|^2 = 0.2$. The analytical steady state results follow the solid and dashed lines. The results of the evolution (stable final states) are given by the solid line and the area bordered by the dotted lines.

Here the intensities are normalized by E_{10}^2, the intensity of both the forward and backward pump waves.

Equation (13) is an elliptic integral of the first kind which can be evaluated using standard techniques. For $l > l_0$, the solution is not unique and this leads to the intriguing possibility of discontinuous transitions between the various steady states. This solution is shown in Fig. 3 (solid and dashed lines). The steady state transmission $|\mathcal{E}_F|^2$ is plotted as a function of medium length l, for equal counterpropagating pump intensities ($E_{10} = E_{20} = 1$). The oscillation threshold would correspond to $l = \pi/2$ in the "negligible pump depletion approximation". The probe is of constant amplitude: $|\mathcal{E}_F(0)|^2 = 0.2$.

In order to verify the stability and existence of the steady state solution, the fields inside the medium were let to evolve with time, according to the system of (7)–(10), with the same boundary conditions as in Fig. 3. The stable equilibrium is found only for the raising portion of the transmission curve (solid line) which agrees accurately with the analytical "steady state" result. The two other analytical steady state solutions (dashed line) found for $|\mathcal{E}_F|^2$ are unstable: given the approximate field configuration of steady state A and B as initial condition ($t = 0$), results in a final steady-state configuration C.

The stability of the solution C against pump power fluctuation and against unbalanced pumps was verified by setting the intensity of the forward pump (E_{10}) to zero for a time interval corresponding to a propagation distance through half the medium thickness.

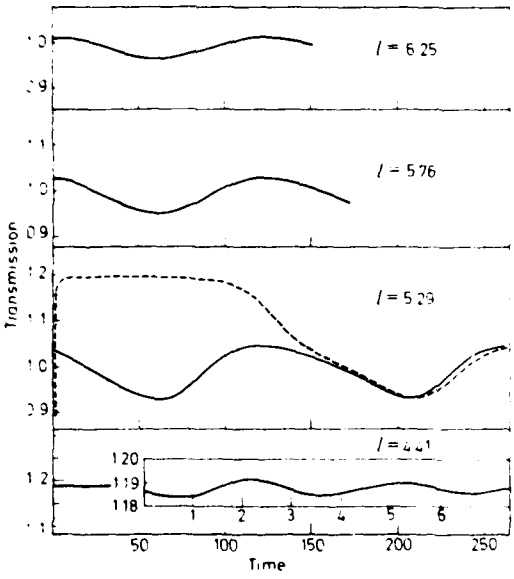

Fig. 4. Evolution with time of the transmission factor $\mathcal{E}_F/\mathcal{E}_{F,0}$ as a function of time for various values of the medium length

The initial perturbation of the fields decayed after a time lapse $t \gtrsim 2l$, and the initial steady state C was recovered. For a medium thickness slightly beyond D, the solution evolve slowly toward periodic oscillation between two states. The amplitude of these oscillations is indicated by the two extreme values of the transmission (Fig. 3, dotted line). As the medium thickness is increased, a true stable steady state is reached again as the two dotted line merge at the intersection (point F) with the dashed line (analytical solution). The field distribution within the medium is monotonic in all cases. The transmission factor $|\mathcal{E}_F(l)|^2$ is plotted in Fig. 4 as a function of time, for various values of the medium length l, in the region of oscillations (dashed area in Fig. 3). As the medium thickness is increased beyond the oscillation threshold D, the period of the oscillations is roughly constant, and surprisingly large compared with the time constants (time for transmission through the medium equal 1) of the system.

We have verified that these solutions are stable, and reached with different initial conditions. An example of an evolution towards final state is shown in Fig. 4, for a medium length $l = 5.3$. A step function probe field is chosen [initial conditions: $\mathcal{E}_F(z) = \mathcal{E}_B(z) = 0$]. The transmission factor initially raises to the value corresponding to an extrapolation of the stable steady solution (solid line in Fig. 3) which appears to be a metastable solution. Thereafter, the transmission factor decreases suddenly to the stable periodic behavior. For even longer media ($l \gtrsim 12$), the field distribution inside the medium ceases to be monotonic. A change of π in the phase factor of the probe beam is seen to propagate periodically from $z = 0$ to $z = l$. In no case did the steady-state solution (dashed line) appear stable. It should be noted that only the nonresonant case $\psi = \pi/2$ can be a candidate for bistable operation. For $\psi = \pi$, two photon absorption always limits the effective length of nonlinear interaction. Based on these time-dependent studies, it appears unlikely that four wave mixing can be used as a multistable device in the case of instantaneous medium response.

Acknowledgement. This work was supported by NSF under grant No. ENG-7826209 and the Office of Naval Research

References

1. A. Yariv, D. M. Pepper: Opt. Lett. **1**, 16 (1977)
2. R. L. Abrams, R. C. Lind: Opt. Lett. **2**, 94 (1978)
3. J. H. Marburger, J. F. Lam: Appl. Phys. Lett. **34**, 389 (1979)
4. J. H. Marburger, J. F. Lam: Appl. Phys. Lett. **35**, 249 (1979)
5. A. Khizhnyak, V. Kondilenko, V. Krementski, S. Odoulov, M. Soskin: OPTEM meeting, Paper 2, Session Opticom 1, Strasbourg, France (1979)
6. D. M. Pepper, D. Fekete, A. Yariv: Appl. Phys. Lett. **33**, 41 (1978)
7. D. Grischkowsky, N. S. Shiren, R. J. Bennett: Appl. Phys. Lett. **33**, 805 (1978)
8. D. G. Steel, R. C. Lind, J. F. Lam, C. R. Giuliano: Appl. Phys. Lett. **35**, 376 (1979)
9. W. W. Rigrod, R. A. Fisher, B. J. Feldman: Opt. Lett. **5**, 105 (1980)
10. D. L. Bobroff, H. A. Haus: J. Appl. Phys. **38**, 290 (1967)
11. B. Ya. Zel'dovich, M. A. Orlova, V. V. Shkunov: Sov. Phys. Dokl. **25**, 290 (1980)
12. H. Winful, J. Marburger: Appl. Phys. Lett. **36**, 613 (1980)
13. J.-C. Diels, Ian McMichael: Opt. Lett. **6**, 219 (1981)
14. J. F. Lam, W. P. Brown: Opt. Lett. **5**, 61 (1980)
15. J. H. Marburger: Appl. Phys. Lett. **32**, 372 (1978)

APPENDIX C

Picosecond Resolution Studies of Ground State Quantum Beats and Rapid Collisional Relaxation Processes in Sodium Vapor

R.K. Jain, H.W.K. Tom[1], and J.C. Diels[2]

Hughes Research Laboratories
3011 Malibu Canyon Road, Malibu, California 90265, USA

[1]Department of Physics, University of California,
Berkeley, California, USA

[2]Department of Physics, North Texas State University,
Denton, Texas, USA

We report experimental studies of coherent transients and collisional relaxation processes in Na vapor, using degenerate four-wave mixing (DFWM) with picosecond pulses. These include investigation of the quantum beat modulation (due to the hyperfine splitting of the ground state) of the intensity of the DFWM signal as a function of excitation pulse separation. The picosecond resolution obtained by varying the pulse delay in our DFWM experiments has resulted in the first observation of harmonic structure in the quantum beat modulation, and in the observation of an anomalously rapid (e^{-1} decay time <50 psec) collisional relaxation process at increased temperatures.

In our experiments, we used the standard DFWM optical arrangement with forward (f) and counter-propagating backward (b) pump pulses, and a probe (p) pulse arriving at the Na cell at times: t_f, t_b, and t_p, respectively. Optical delay lines allowed us to vary both t_p and t_b independently with respect to t_f, whose instant of arrival is defined here as the zero reference of time. For our excitation source, we used ~35 psec pulses ($\Delta\nu$ = 9.5 GHz) at 5890Å (D_2-line) from a cw Rn 6G dye laser synchronously-pumped by a mode-locked Ar^+ laser (repetition rate ~80 MHz). DFWM signals were easily observed and the average power in the signal wave (i.e., the energy in the signal pulse) was monitored with a slow photodiode and phase-sensitive (~1 MHz) detection electronics. In contrast with other related work [1-3], no cavity dumping or amplification of the output of the cw mode-locked dye laser was used for these experiments, and pulse areas were typically less than $\pi/100$. A Faraday isolator was used to prevent feedback into the dye laser.

In Fig. 1, we show the signal intensity as a function of t_p, with t_b fixed at values of 1670 psec and 370 psec. The signal intensity is plotted on a logarithmic scale, to emphasize the dynamic range of the data in the region of fast decays, such as $t_p < 0$. The modulation of the signal in both figs. 1a and 1b at both the fundamental and second harmonic of the ground state hyperfine frequency (ν_{12} = 1.77 GHz, T_{12} = 565 psec) is easily observable. In the special case in which pulses are incident in the sequence f,p,b (i.e., $0 < t_p < t_b$), the four-wave mixing signal has been identified as a photon echo (called the backward-wave echo) with emission occurring at $t=t_p+t_b$ [1,4]. No echo occurs for $t_p < 0$, or for $t_p > t_b$. Quantum beat modulation in the echo itself has been discussed by Nakatsuka, et al., but this is the first experimental study of quantum beat modulation of the pulse energy as a function of excitation pulse separation times. Characterizing this quantum beat modulation is essential before ultrashort pulses can be used for DFWM studies of rapid relaxation processes, such as for the study of the effect of dephasing or rephasing collisions with a large number of external perturbers.

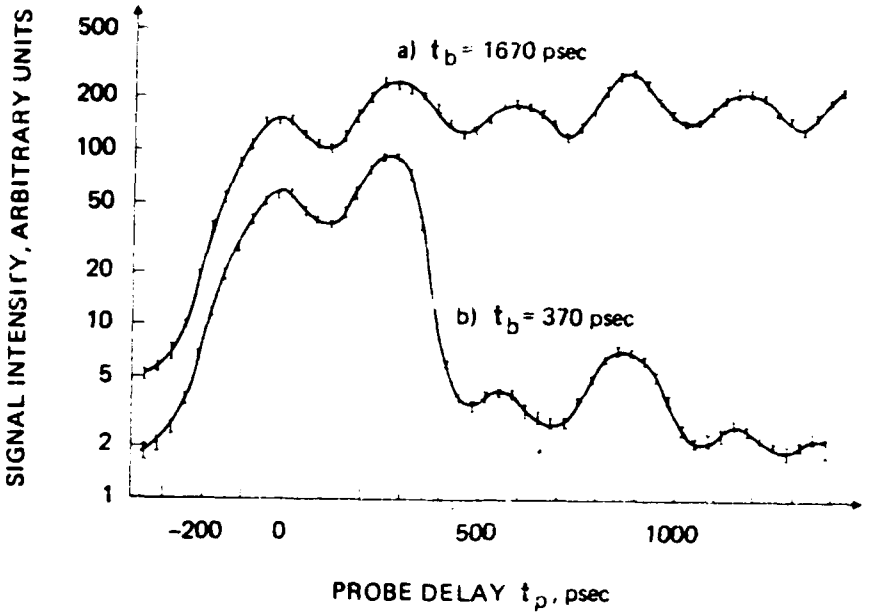

Fig.1 Signal intensity vs. t_p at two values of the delay t_b and at fixed cell temperature. The relative magnitude of the curves is not significant.

The rapid decay of the signal in Fig. 1b, at $t_p \sim 370$ psec, is due to the change in the pulse sequence. This rapid decay is consistent with the absence of the photon echo, and was verified by noting rapid decays at the appropriate time delays t_p for various other choices of t_b. The modulation in the signal for $t_p > t_b$ is attributed to subsequent backward pulses (from the high repetition $_{rate}$ laser) scattering off the ν_{12} modulated spatial grating formed by an initial f-p pulse pair.

It is well established that transient four-wave mixing in the backward-wave echo geometry is a useful probe of relaxation processes affecting single states and coherent superpositions of states [1,4]. In Fig. 2, we show evidence of an ultrafast collisional relaxation process that we observed at increased temperatures. 250 mTorr of He buffer gas was used for the data of Fig. 2(a). Such a strong temperature dependence and anomalously rapid decay is not directly attributable to known cross sections of Na-He and Na-Na collisions. In the absence of He buffer gas (see Fig. 2(b)), similar decays were observed at slightly higher (~15°C) temperatures, excluding the possibility of relaxation via Na-He collisions. One possible source of such behavior is an unknown impurity, perhaps due to outgassing from the specific cells used; we are presently unaware of an impurity with such a large Na-perturber cross section. This rapid decay is presently a topic of further investigation [6].

In our talk, we will compare our experimental observations with theory. The relation between quantum beats observed in our backward-wave echo experiments and quantum beats observed in fluorescence [5] and transmission [2] experiments will be discussed.

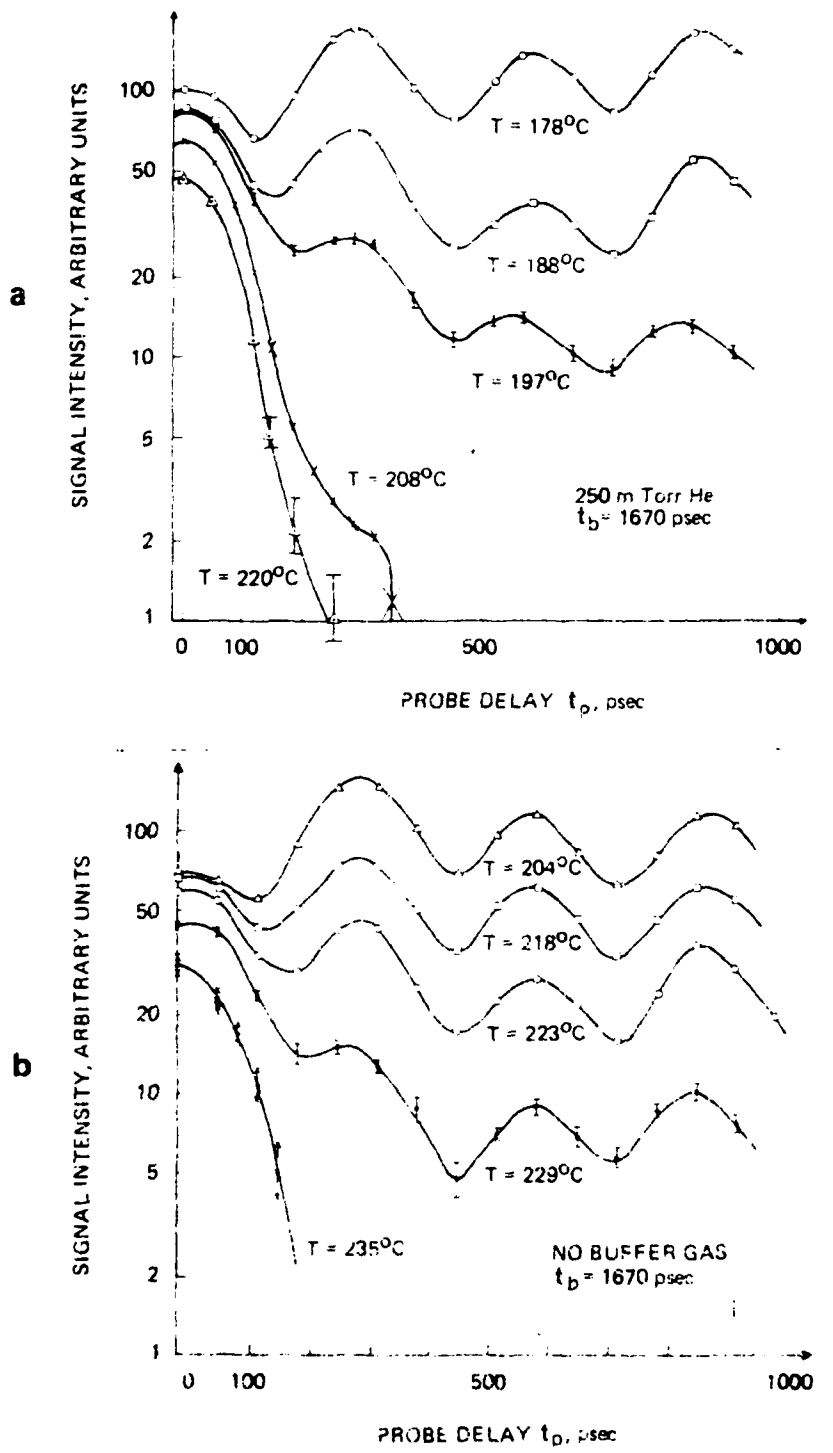

Fig.2 Signal intensity vs. t_p at fixed t_b and different values of the cell temperature. For Fig. 2(a), 250 mTorr of the buffer gas was also present in the cell.

References

1. M. Fujita, H. Nakatsuka, H. Nakanishi and M. Matsuoka, Phys. Rev Lett. 42, 974 (1979).
2. H. Harde, H. Burggraf, J. Mlynek and W. Lange, Optics Lett. 6, 290 (1981).
3. H. Nakatsuka, M. Fujita and M. Matsuoka, Optics Comm. 36, 234 (1981).
4. T. Mossberg, A. Flusberg, R. Kachru and S.R. Hartmann, Phys. Rev. Lett. 42, 1665 (1979).
5. S. Haroche, in High-Resolution Laser Spectroscopy, ed. K. Shimoda, Springer-Verlag, New York (1976).
6. Another possible mechanism for this rapid decay is the associative ionization of the sodium from the laser-excited $3P_{3/2}$ states. For instance, see: F. Roussel, B. Carré, P. Brewer, and G. Spiess, J. Phys. B14, L313 (1981); A. de Jong and F. van der Valk, J. Phys. B12, L561 (1979).

SUBPICOSECOND PULSE SHAPE MEASUREMENT AND MODELING OF PASSIVELY MODE LOCKED DYE LASERS INCLUDING SATURATION AND SPATIAL HOLE BURNING

J.-C. Diels, I. C. McMichael
Center for Applied Quantum Electronics, North Texas State University
Denton, TX 76203
J. J. Fontaine ENSAIS and LSOCS
Universite Louis Pasteur, Strasbourg, France
and
C. Y. Wang
Tientsin University, Optical Department
Tientsin, The Peoples Republic of China

1. Introduction

We present a theoretical model of the linear and ring, passively mode locked dye lasers. This simple model gives a clear understanding of the role of the amplifier, the absorber, and the dynamics of the degenerate third order nonlinearity resulting from spatial hole burning [1].

The validity of the model is established by fitting the pulse shapes measured experimentally in the case of the linear laser. The model predicts a minimum pulse duration in the case of the ring laser which is within a factor of two of that obtained in experiments [2].

2. The Experimental Measurement of the Pulse Shape

In each roundtrip time for the linear cavity (4 ns) we observe a train of two pulses separated by 0.33 ns. The 0.33 ns corresponds exactly to the roundtrip time for pulses to travel from the dye jet, to the end mirror, and back to the jet. This indicates that the pulses must collide in the jet.

Two aspects of the linear laser output make it possible to extract information about each of the two pulses from the auto- and cross-correlations. First, since the peak intensity of the first pulse in the train of two is more than 15 times that of the second, the auto-correlation near zero delay is unaffected by the second pulse. Second, since the second pulse in the train of two is much broader than the first, the cross-correlation accurately portrays the shape of the second pulse.

The experimental measurements are shown in Fig.1. The front of the broad weak pulse has a slow rise followed by a fast decay. The auto-correlation of the sharp intense pulse scaled down to the peak amplitude of broad weak pulse is indicated by the dashed line.

3. The Theoretical Model

The theoretical model includes saturation of the gain and absorbing media, interaction of the pulses through spatial modulation of the populations of the active media, a finite jet thickness, and dispersion and bandwidth limitation in the cavity. The population difference W of either media will evolve according to the rate equation

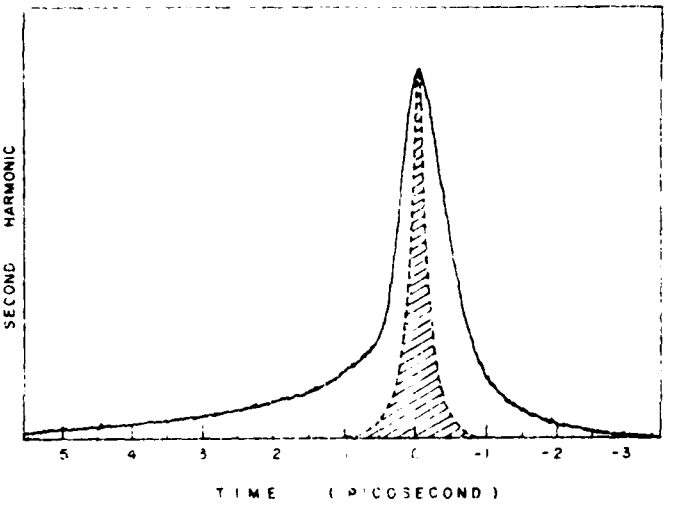

Fig.1 Cross-correlation: shape of the weak pulse

$$\dot{W} = -\left\{\frac{E^2}{E_s^2}\, W + (W - W_{eq})\right\}/T_1 \quad . \tag{1}$$

In Eq. 1 E_s is the saturation field, W_{eq} is the population difference in the absence of fields, and T_1 is the lifetime (corrected for the pumping rate in the case of the amplifying medium). With a driving field E composed of two counterpropagating components

$$E = \mathcal{E}_1\, e^{i(\omega t - kz)} + \mathcal{E}_2\, e^{i(\omega t + kz)}$$

the population differences will be of the form

$$W_j = W_{0j} + W_{2j}\, e^{2ikz} + W_{2j}^*\, e^{-2ikz}$$

with j = G for the gain medium, and j = A for the absorber.

For propagation in the dye jet the equations are written in advancing spatial coordinates for $\mathcal{E}_1$ and regressing spatial coordinates for $\mathcal{E}_2$.

$$\dot{\mathcal{E}}_1 = A_0\, \mathcal{E}_1 + A_2\, \mathcal{E}_2$$

$$\dot{\mathcal{E}}_2 = A_0\, \mathcal{E}_2 + A_2^*\, \mathcal{E}_1$$

A_0 includes contributions from the W_{0j}'s and A_2 includes contributions from the W_{2j}'s. One should not forget while looking at these equations that the A's are functions of the fields. The media comprising the dye jet are allowed to relax between pulse passages. At each cavity roundtrip the fields are modified to account for the spectral narrowing and dispersion introduced by the mirrors and solvent in a real cavity. Arbitrary shapes are assumed for $\mathcal{E}_1$ and $\mathcal{E}_2$ and then the calculation is cycled until a steady state is reached.

4. Discussion and Results

Figure 2 shows the calculated pulse shapes for the two pulses in the linear laser. The slow rise and rapid decline of the weak pulse appears as in the experiment. Inspection of the numerical values of $W_{2j}(t)$ indicate the formation of a strong grating during the slow rise of the weak pulse. As the peak of the strong pulse is approached, the population gratings are washed out by complete saturation. It should also be noted that the pulse shapes are nearly independent of the jet thickness, but strongly affected by dispersion.

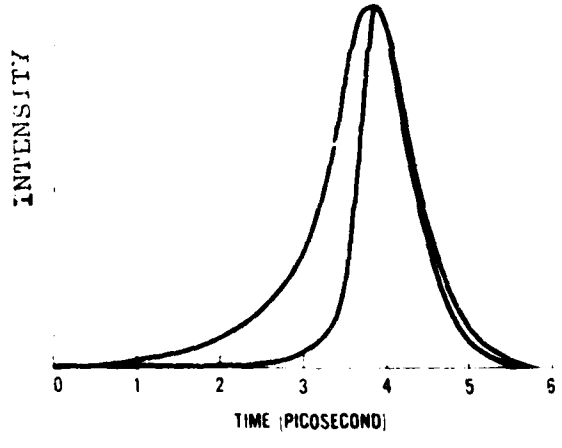

Fig.2 Calculated pulse shapes for the linear laser

This same model was used to describe colliding pulse mode locking in the ring laser. The only differences from the previous calculations are in the sequence of events and the fact that mutual interaction of the counter propagating pulses occurs only in the absorber jet. A steady state pulse shape is shown in Fig.3. Unlike the calculation for the linear laser, the calculation for the ring laser indicates that in the absence of dispersion the pulse duration is limited by the jet thickness. For this figure the medium thickness was 120 μm. The pulse duration corrected for medium dispersion is 0.4 psec in air. Scaling the thickness down to 10 μm yields a minimum duration of 35 ftsec. This is within a factor of two of the result obtained by FORK et al. [2].

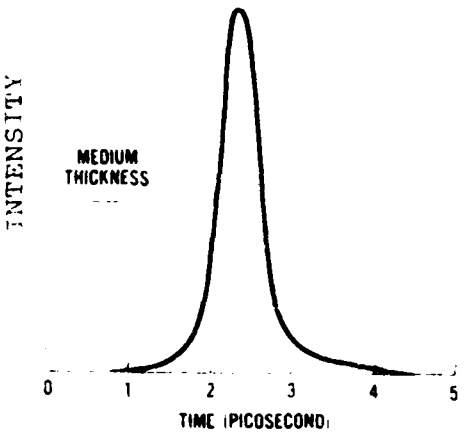

Fig.3 Calculation for the ring laser

5. Conclusions

A theoretical model has been made which describes the pulse forming mechanism in passively mode locked dye lasers. The model includes those parameters that are essential to the operation of the laser. The exact influence of each parameter has been evaluated by fitting the experimental data from a linear cavity.

In the case of the linear laser the model predicts that the pulse shape is independent of the dye jet thickness and that a population grating is formed in the leading edge of the broad weak pulse. In the case of the ring laser the model predicts that the pulse shape is dependent on jet thickness, that the induced grating yields pulse broadening, and that the stable regime results from a balance between pulse broadening and pulse compression by mutual saturation.

The agreement between these predictions and the results of experiment leads us to conclude that the proposed model accurately describes the colliding pulse mechanism in passively mode locked linear and ring lasers.

This work was supported by the National Science Foundation, Grant No. ECS-8119568, and the Office of Naval Research.

REFERENCES

1. J.-C. Diels, and W. C. Wang, Applied Phys. B 26, 105 (1981); R. L. Adams and R. C. Lind, Opt. Lett. 2, 95 (1978); J. B. Hambenne and M. Sargent, IEEE J. Quant. Elect. QE-11, 90 (1975).
2. R. L. Fork, B. I. Greene, and C. V. Shank, Applied Physics Letters 38, 671 (1981).

APPENDIX E

DEGENERATE FOUR WAVE MIXING OF PICOSECOND PULSES IN THE SATURABLE AMPLIFICATION OF A DYE LASER

J.-C. Diels, I. C. McMichael, and H. Vanherzeele
Center for Applied Quantum Electronics
Department of Physics
North Texas State University
Denton, Texas 76203

ABSTRACT

We demonstrate intracavity degenerate four wave mixing in the saturable gain medium of a dye laser. The dye laser is a synchronously pumped bidirectional ring laser that produces pulses of 4 ps duration. The dynamics of the interaction provides information on the phase coherence of the pulses. A simple theory of transient degenerate four wave mixing is presented that accurately describes the measurements.

1. Introduction

Degenerate four wave mixing (DFWM) has been proposed and used extensively to generate phase conjugated reflected signals. More than 100% reflection has been demonstrated by this method. However, high reflectivities are generally incompatible with fast response times. It has been demonstrated by Diels et al.[1] that simultaneous temporal and spatial phase conjugation requires that the medium thickness be smaller than the length of optical fluctuations. In addition, the medium should be optically thin--i.e., the relative change in any of the signals sent into the media should be small (for instance the probe amplification). This last condition eliminates the possibility of simultaneous efficient temporal and spatial phase conjugation by degenerate four wave mixing. Fast temporal phase conjugation is important for some potential practical applications. For instance, we proposed fast response temporal phase conjugation by DFWM in laser gyros,[2] to reduce the lock-in effect, and to extend the palette of gyro laser candidates to lasing media with mutual saturation (all homogeneously broadened lasers). For that particular application, the response time should at least exceed the GHz range.

The saturation of organic dyes offers a possible solution to the problem of fast and efficient DFWM, because it is a broadband nonlinearity that can be used in continuous operation. The dye bandwidth makes application up to THz conceivable. The requirement of "thin media" is also met (up to 10 THz) in thin dye jets. The saturation can be that of an absorber or of an amplifier. In this paper we consider the latter case.

To date there are only a few demonstrations of degenerate four wave mixing (DFWM) in amplifiers.[3] In these experiments comparison is made with the steady state treatment of DFWM developed by Abrams and Lind.[4] We present the first demonstration of DFWM of picosecond pulses in a saturable amplifier. Our

theoretical model, accounting for the transient nature of the interaction, provides an accurate match to the experimental data.

2. Experimental Set-Up

The experimental set-up is shown in Fig. 1. A Rhodamine 6G ring dye laser is synchronously pumped by an actively mode-locked argon ion laser with a maximum average power of 2.6 W at 514 nm. The ion laser produces a train of pulses of approximately 125 ps duration at a repetition rate of 245 MHz. The dye jet is the nonlinear medium in which the counterpropagating pulses of the laser provide the pump beams for DFWM. A synchronously pumped ring laser configuration is essential to insure mutual coherence of the counterpropagating laser pulses at the dye jet.[5] In any other mode of operation, we were unable to observe DFWM. For instance, with continuous pumping, the dye laser could be operated continuously or passively mode locked, by mixing a saturable absorber with the amplifying dye solution. In either mode of operation, the lack of mutual coherence between the counterpropagating pulses at the dye jet was confirmed by a simple experiment of linear interferences. When both outputs of the ring laser were superimposed at a point equidistant from the dye jet (Fig. 1b), no interference fringes could be observed. We believe that the lack of mutual coherence at the dye jet results from the strong competition of the counterpropagating beams through mutual saturation of the gain medium.[2]

Efficient DFWM requires that the optical density of the nonlinear medium be as large as possible.[1] To ensure a maximum nonlinearity, the energy density of the counterpropagating laser pulses in the gain medium should be of the order of the saturation energy density. These conditions call for a ring cavity with large linear losses. Therefore, we use a 33% transmission output coupler, and insert a neutral density filter of optical density ND = 0.3 in the laser resonator.

Second order autocorrelations indicate that the ring laser produces pulses of 4 ps duration. One of the laser outputs provides the probe beam for DFWM (Fig. 1a). The technical difficulty of superimposing the pump and probe beams in the dye jet was solved by imaging the dye jet fluorescence and a probe beam reflection on a distant screen. A monochromator with a bandwidth of 1 nm, set to the laser wavelength, is used to discriminate against the strong fluorescence background that is imaged near the return (signal) beam. Alignment of the signal detection involves the use of a mirror to retroreflect the probe beam for accurate positioning of the monochromator and detection assembly. After this mirror is removed, the optical delay of the probe beam is adjusted by translating the retroreflecting prism (Fig. 1a) until a maximum return signal is detected by the photomultiplier tube (RCA 4832). Direct viewing of the DFWM signal is accomplished by replacing the monochromator by a dispersive prism.

A reference for 100% reflectivity is obtained by retroreflecting the probe beam into the detection system with a mirror placed after the beam splitter. We use calibrated neutral density filters to attenuate the return beam to levels obtained in the DFWM. In order to check the accuracy of this procedure against possible errors in imaging, the calibration measurement was verified using a large area silicon photodetector, and narrow band interference filters. The measurements agreed to within 3%.

3. Determination of the Saturation Energy

Since saturation is the nonlinear mechanism involved in this form of DFWM, an accurate knowledge of the pulse energy required to saturate the gain medium is necessary in order to make quantitative comparison of the experimental results with the theory. From simple four level laser theory[6] we obtain an expression for the saturation energy W_sA (A being the cross section of the beam) in terms of other laser parameters,

$$W_s A = \frac{\lambda_p}{\lambda_\ell} \frac{Q}{2\alpha_s \ell} P_{th} T_1 \qquad (1)$$

λ_p, λ_ℓ are the pump and laser wavelengths (514.5 nm and 570 nm), Q is the quantum efficiency (0.95 for Rhodamine 6-G),[7] T_1 is the excited state lifetime (3.3 ns for Rhodamine 6-G),[8] $e^{-2\alpha_s \ell} = 0.33$ is the loss per cavity roundtrip (no neutral density filter was used for this measurement), and P_{th} is the absorbed pump power necessary to achieve threshold. Our cw pumping threshold for 33% output coupling was 480 mW. Using our laser parameters, we obtain a saturation energy of 3.4 nJ.

The saturation energy can also be calculated directly from the spot size in the gain medium and the saturation energy density,

$$W_s = \frac{h\nu}{\sigma} \qquad (2)$$

where h is Planck's constant, ν is the light frequency, and σ is the emission cross section. Using a value of $3 \times 10^{-16} cm^2$ for the stimulated emission cross section of Rhodamine 6-G at 570 nm,[9] yields a saturation energy density of 12 $pJ/\mu m^2$. With an estimated spot size of 20μm, we obtain a saturation energy of 3.7 nJ in good agreement with our previous value.

4. Measurements of DFWM

With the probe delay set at its optimum position (Fig. 1) corresponding to a maximum reflectivity, we measure the DFWM signal as a function of pump intensity. Fig. 2 shows the corresponding plot of the measured reflectivity versus the ratio of the pump pulse energy to the saturation energy. Error bars indicate the rms fluctuations in the measurements. The curve is a theoretical fit using only the saturable gain/pass exp $2(\alpha_s \ell)$ as an adjustable parameter (cf section 5).

Data could only be taken over a limited range of energies due to unstable operation of the laser at the extreme ranges of pumping. At low energies the laser became unstable due to operation near threshold. At high energies the mode locking became unstable as evidenced by the display of a real time autocorrelator. Following Steel, Lind, and Lam,[10] we have made a phenomelogical correction to the measured pump pulse energy to account for gain in the dye jet. The energies are corrected by a factor $e^{2\alpha_s(\ell/2)}$, where $2\alpha_s\ell$ is the saturated gain coefficient for the intensity.

Within the range of available data in Fig. 2, the complicated functional dependence detailed in section 5 fits a straight line of slope 2.1. By approximating the data by a slope 2, we can associate a third order nonlinear susceptibility χ_3 with the saturated DFWM. Consequently, the nonlinear susceptibility tensor $\chi(E)$ defined by

$$P_1 = \varepsilon_0 \chi(E)\, E \tag{3}$$

where P_1 is the total polarization and E the total field, can be replaced by a scalar third order susceptibility χ_3 such that the signal polarization amplitude $\mathcal{P}_s$ is given by

$$\mathcal{P}_s = \varepsilon_0 \chi_3 \mathcal{E}_1 \mathcal{E}_2 \mathcal{E}_p \tag{4}$$

where $\mathcal{E}_1$ and $\mathcal{E}_2$ are the amplitudes of the counterpropagating pump fields, and $\mathcal{E}_p$ is the probe amplitude. Using the notations of ref. 1 (Eqs. 6-12) and a linear approximation for the propagation through the jet of thickness ℓ, the signal field is given, in MKS units, by

$$\mathcal{E}_s = \frac{i\omega\chi_3}{2C}\,(\mathcal{E}_1\mathcal{E}_2\mathcal{E}_p)\ell \tag{5}$$

Eq. (5) leads to a reflection coefficient which is the ratio of the signal intensity to the probe intensity, that can be fitted to Fig. 2:

$$R = \left| \frac{\mu\omega}{2} \chi_3^{\ell} \frac{W_p}{\tau} \right|^2 = 0.79 \left| \frac{W_p}{W_s} \right|^2 \qquad (6)$$

In Eq. (6), W_p is the probe pulse energy density, W_s the saturation energy density (12 J/m^2), τ the pulse duration (4 psec), μ the medium permeability. The right side of Eq. (4) is a quadratic fit of Fig. 2. Eq. (4) yields a nonlinear susceptibility of $\chi_3 \approx 10^{-18} m^2/V^2$, a value 500 times larger than that of CS_2.

Fig. 3 shows a measurement of the DFWM signal versus the probe delay. The width of the recording (0.6 ps FWHM) is much less than the pulse width as determined from intensity autocorrelations. Interferometric autocorrelations[11] indicate that the 0.6 ps corresponds to the coherence time of the train. Since no coherence spike is observed in the conventional intensity autocorrelation with a peak to background ratio of 3 to 1, one has to conclude that the 0.6 ps corresponds to a phase coherence time. It should be noted, however, that autocorrelation traces cannot distinguish an ensemble feature from that of a single pulse. That is, the phase coherence of 0.6 ps for a train of 4 ps pulses could either indicate that each individual pulse is phase modulated, or that pulses of the train have different frequencies. This ambiguity is removed by the DFWM measurement, which indicates a phase coherence of only 0.6 ps for each individual pulse. Indeed, in DFWM the three waves have to be mutually coherent in order for one of them to diffract off the population grating formed by the two others. This condition can only be fulfilled for a range of delays corresponding to the coherence time of the laser. In this particular scheme of

synchronous pumping, this phase coherence time coincides with the light transit time through the jet. We can therefore conclude that the response time of this type of DFWM is approximately 0.5 ps. An important consideration, as discussed in section 6, is the susceptibility-bandwidth product, which compares favorably with any other nonlinear device at that wavelength.

5. Theoretical Analysis

Analysis of steady state DFWM in saturable amplifiers was presented by Reintjes and Palumbo.[12] This steady state approach does not apply to the present experimental condition, since we are using pulses much shorter than the energy relaxation time. Numerical solution of the transient response of DFWM in resonant saturable absorbers was obtained by Silverberg and Bar-Joseph.[13] With a similar model adapted to a dye amplifier, we obtain analytical solutions of the transient response of DFWM with short pulses (pulse duration, τ, much less than the population relaxation time T_1) in absorbing and amplifying media. We find that in the case of short pulses $\tau \ll T_1$ the DFWM reflectivity depends only on the optical density of the saturable medium and the energy of the pulses and is independent of the pulse duration. In the usual plane wave approximation, the four fields

$$E_i(r,t) = \frac{1}{2}\mathcal{E}_i(r_i)\exp[i(\omega t - \vec{k}_i \vec{r})] + \text{c.c.} \qquad r_i = \frac{\vec{k}_i \cdot \vec{r}}{|\vec{k}_i|} \qquad (7)$$

interact in a nonlinear medium. We consider the case of counterpropagating pump waves of equal amplitudes $\mathcal{E}_1 = \mathcal{E}_2$. $\mathcal{E}_3(0,t)$ is the amplitude of the return signal counterpropagating (in the Z-direction) to the probe $E_4(0,t)$.

For an absorbing or amplifying transition in which the final state quickly relaxes to some other state, the population of the initial state changes for

times $t \ll T_1$, according to the rate equation,

$$\dot{N} = -\frac{I}{W_s} N \tag{8}$$

where I is the intensity of the interacting fields and W_s is the saturation energy density. For a step function excitation $\mathcal{E}_0$, the relevant population N, changes with time according to

$$\frac{N(W)}{N_0} = (\exp - W) \tag{9}$$

where $W = It/W_s$, and N_0 is the equilibrium population of the initial state in the absence of saturating fields. On resonance, the susceptibility defined by Eq. 1 is given by

$$\chi = i \frac{2\alpha_0}{k} \frac{N(W)}{N_0} \tag{10}$$

where α_0 is the small signal field gain (absorption) coefficient and k is the wave number. Expanding the susceptibility to first order in the weak fields $\mathcal{E}_{3,4}$ gives,

$$\chi = i \frac{2\alpha_0}{k} e^{-2W_T \cos^2\theta} \left[1 - \frac{t}{W_s} 2\mathcal{E}_1 \cos\theta \left(\mathcal{E}_3 e^{-ikz} + \mathcal{E}_4 e^{ikz} + cc\right)\right] \tag{11}$$

where $W_T = 2W/W_s$ is the total energy from the pump fields normalized to the saturation energy and $\theta = \vec{k_1} \cdot \vec{r}$.

Substitution of Eq. (11) into the wave equation, with the polarization (3), gives the coupled amplitude equations in the slowly varying amplitude approximation,

$$\frac{d\mathcal{E}_3}{dz} = \alpha_0 (\mathcal{Y}_1 \mathcal{E}_3 - \mathcal{Y}_2 \mathcal{E}_4^*)$$

$$\frac{d\mathcal{E}_4}{dz} = -\alpha_0 (\mathcal{Y}_1 \mathcal{E}_4 - \mathcal{Y}_2 \mathcal{E}_3^*) \tag{12}$$

where, on averaging over the spatial dependence of $\mathcal{Y}_1$ and $\mathcal{Y}_2$, we obtain,

$$\mathcal{Y}_1 (W_T) = [(1-W_T)\, I_0 (W_T) + W_T\, I_1 (W_T)] \exp (-W_T)$$
$$\mathcal{Y}_2 (W_T) = [I_0 (W_T) - I_1 (W_T)]\, W_T \exp (-W_T) \tag{13}$$

where I_0 and I_1 are the modified bessel functions. For one input probe $\mathcal{E}_4(0)$, $\mathcal{E}_3(\ell) = 0$, the reflectivity,

$$R = \left| \frac{\mathcal{E}_3 (0)}{\mathcal{E}_4 (0)} \right|^2 \tag{14}$$

is obtained from the coupled amplitude eqs. (12).

$$R(\alpha_o \ell, W_T) = \left| \frac{y_1}{y_2} - \frac{\sqrt{y_1^2 - y_2^2}}{y_2} \coth \left(\alpha_o \ell \sqrt{y_1^2 - y_2^2} \right) \right|^{-2} \qquad (15)$$

For square pulses the average reflectivity is

$$\langle R \rangle = \frac{1}{2 W_p} \int_0^{2 W_p} R(\alpha_o \ell, W_T)\, d W_T \qquad (16)$$

where W_p is the energy of each pump pulse normalized to the saturation energy. Fig. 6 shows plots of Log R versus Log W_p. Bold lines are for an amplifier $\alpha_o \ell = +1$ and dashed lines are for an absorber $\alpha_o \ell = -1$. In each plot, the small signal gain is maintained constant. The steady state results are based on the theory of Abrams and Lind. For these lines the abscissa is Log I/I_s, where I/I_s is the intensity of the pumping fields normalized to the saturation intensity. The results for $T = T_1$ are based on the theory of Silberberg and Bar Joseph. The results for short pulses, $\tau << T_1$, are based on eq. (16). These plots indicate that DFWM is most efficient in amplifiers, the maximum reflectivity being one order of magnitude larger than for the absorber. They also show that the maximum reflectivity is obtained for short pulses. The dependence of the maximum reflectivity on pulse duration is most pronounced in the absorber.

The curve fitting for Fig. 2 was made using the eqs. 13-16. As in the experimental situation, the saturated gain factor $\exp(\alpha_s \ell)$ which is equal to the combined losses at the output mirror and neutral density filter, is set to be constant. This saturated gain factor is used to calculate, for each pump power, the value of the small signal gain, which is inserted in Eqs. 13-16. The curve of Fig. 2 used the saturated gain factor/pass as only fitting parameter.

The best fit $\alpha_s{}^{\chi} = 0.44$ corresponds to 80% of the measured value.

Relaxation from the final state of the resonant transition could produce thermal phase gratings that contribute to the four wave mixing. The DFWM reflection due to a thermal grating should have a temperature dependence, since the thermal conductivity of the Rhodamine 6G solution is temperature dependent. We could not observe any such temperature dependence in the range of 0°C to 26°C. The excellent fit of our data to a model based on saturation alone indicates that the thermal effect is much smaller than that of saturation in the resonant amplifier.

6. Comparison with other Nonlinearities

It is difficult to make a rigorous comparison of various schemes of DFWM, because of the different nature of the interaction. In several cases such as this one, a third order susceptibility can be defined for a certain range of field intensities. Comparisons should take into account the wavelength and the response time, since the nonlinearities generally increase with wavelength and large susceptibilities are generally associated with long response times. A few materials for DFWM are listed in Table 1, with the corresponding third order susceptibility.

Material	$\chi_3 m^2/V^2$	Wavelength μm	Ref.
Si	$0.9\ 10^{-16}$	1.06	14
Ge	$4.0\ 10^{-20}$	4.0	15
CS_2	$2\ 10^{-21}$	0.7	16
Rh6G (Gain)	10^{-18}	0.57	this work
GaP	$2\ 10^{-18}$	0.53	17

TABLE 1

Some solid state nonlinearities are larger than that of the Rh6G gain jet (for instance, Si and GaP). None of these however can handle, in continuous

operation, a comparable average power density.

Comparing the amplifier with the saturable absorber, our study shows that the return signal can be an order of magnitude larger in the former. It should be pointed out, however, that the strong fluorescence background in the case of the amplifier may be a serious handicap for many potential applications.

7. Conclusions

We have used the counterpropagating beams in a synchronously mode locked ring dye laser as "pump beams" to study DFWM in an amplifying dye jet. A theoretical model based on transient saturated amplification accurately matches the data. Our data emphasize the importance of light coherence in DFWM. It is shown that the experiments performed here provide a diagnostic for mode locked lasers that complements interferometric autocorrelations. In the latter, an average coherence of the pulse train (made of individual pulse coherence and pulse to pulse fluctuations), is measured, while the DFWM experiment provides coherence information on each single pulse.

We have shown that the maximum DFWM is one order of magnitude larger for saturable amplifiers than for saturable absorbers.

This work was supported by the Office of Naval Research and the National Science Foundation under grant number ECS 8119568.

REFERENCES

1. J.-C. Diels and W. C. Wang, "Dynamics of the nonlinear four wave mixing interaction," Appl. Phys. vol. B 26, pp. 105-110 (1981).

2. J.-C. Diels and I. C. McMichael, "Influence of wavefront conjugation coupling on the operation of a laser gyro," Opt. Lett. vol. 6, pp. 219-221 (1981).

3. A. Tomita, "Phase conjugation using gain saturation of a Nd:YAG laser," Appl. Phys. Lett. vol. 34, pp. 463-464 (1979); R. A. Fisher and B. J. Feldman, Opt. Lett. 4, 140-142 (1979).

4. R. L. Abrams and R. C. Lind, "Degenerate four wave mixing in absorbing media," Opt. Lett. vol. 2, pp. 94-96 (1978); "Errata," Opt. Lett. 3, 205 (1978).

5. J. P. Heritage and E. D. Isaacs, "Subpicosecond pulse generation in a synchronously mode-locked bidirectional ring laser," IEEE J. Q. E. vol.17 #12, pp. 52-54 (1981).

6. A. Yariv, "Optical Electronics" (Holt, Rinehart and Winston, 1976), pp. 121-124.

7. F. P. Schäfer, "Dye Lasers" (Springer-Verlag, 1973), p. 149.

8. M. D. Fayer, Third Topical Meeting of Picosecond Phenomena, paper FA3, Garmisch Partenkirchen; proceedings in Picosecond Phenomena III, Springer-Verlag, pp. 82-86 (1982).

9. P. Hammond, "Comparison of experimental and theoretical excited state spectra for Rhodamine 6G," IEEE J. Q. E. vol. 16 #11, pp. 1157-1160 (1980).

10. D. G. Steel, R. C. Lind, and J. F. Lam, "Degenerate four wave mixing in a resonant homogeneously broadened system," Phys. Rev. A vol. 23, pp. 2513-2524 (1981).

11. J.-C. Diels, J. Menders, and H. Sallaba, "Generation of coherent pulses of

60 optical pulses through synchronization of the relaxation oscillations of a mode-locked dye laser," Picosecond Phenomena II (Springer-Verlag, 1980), pp. 41-45.

12. J. Reintjes and L. J. Palumbo, "Phase conjugation in saturable amplifiers by degenerate frequency mixing," IEEE J. Q. E. vol. 18, pp. 1934-1939 (1982).

13. Y. Silberberg and I. Bar-Joseph, "Transient effects in degenerate four wave mixing in saturable absorbers," IEEE J. Q. E. vol. 17, pp. 1967-1970 (1981).

14. R. K. Jain, M. B. Klein, and R. C. Lind, "High efficiency DFWM of 1.06 m radiation in silicon," Opt. Lett. vol. 4, pp. 328-330 (1979).

15. D. Depatic and D. Haneisen, "Multiline phase conjugation at 4 m in Ge," Optics Lett. vol. 5, pp. 252-254 (1980).

16. A. Yariv, "Phase conjugate optics and real time holography," IEEE J. of Quantum Elec., vol. QE-14, pp. 650-660 (1978).

17. W. Sibbett and J. R. Taylor, "Phase-conjugate reflection through DFWM in gallium phosphide," Optics and Quantum Electronics, vol. 16, pp. 81-84 (1982).

FIGURE CAPTIONS

1a. Experimental Set Up. The ring laser cavity is closed by the mirrors M1, M2, M3 and M4. The amplifying dye jet is pumped by an Argon ion laser beam (not shown). One output of the dye laser is retroreflected by the prism P1 (delay adjustment), and sent as probe beam into the dye jet via a beam splitter (BS) and mirrors M5-M6. The signal beam is filtered by the monochromator P2-S and detected by a RCA 4832 photomultiplier tube.

1b. Mutual coherence of the counterpropagating beams: The two output beams are made to interfere on a screen. The position of the prism P is adjusted to make the optical paths from M4 to the screen equal to the optical distances of M4 to the jet.

2. Reflectivity versus normalized Pump Pulse Energy

3. DFWM Signal versus Probe Pulse Delay

4. Reflectivity as a function of pulse intensity for various pulse durations. The abcissa are the intensity normalized to the saturation intensity I_s (steady state curve), or the pulse energy normalized to the saturation energy.

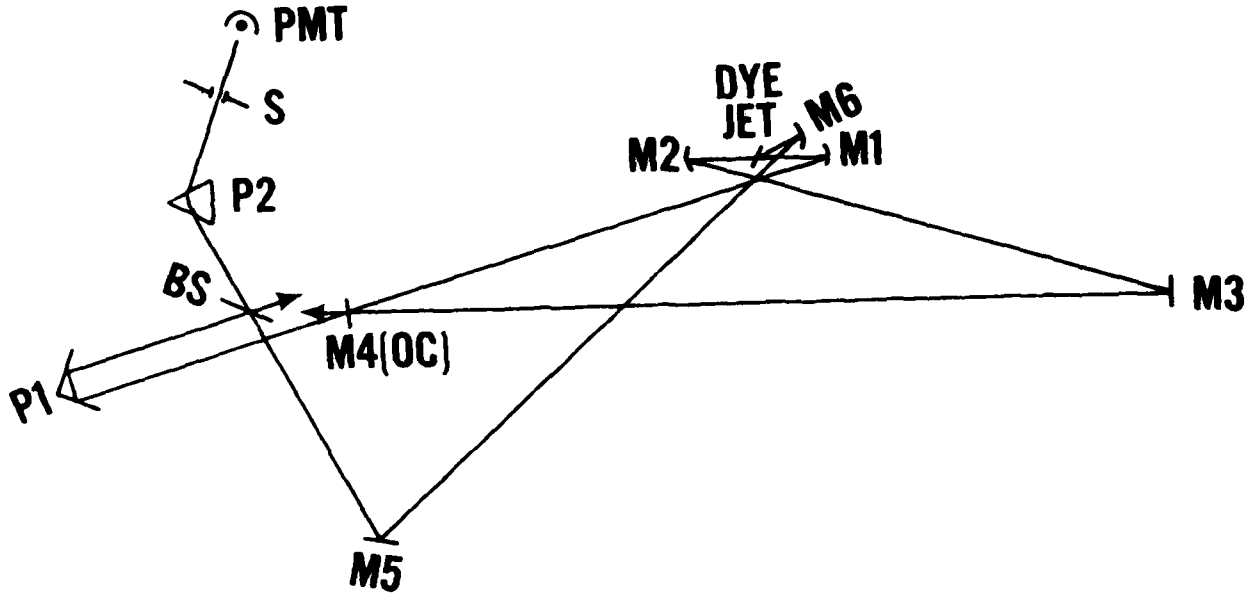
PMT
S
P2
BS
P1
M4(OC)
M5
DYE
JET
M6
M2
M1
M3

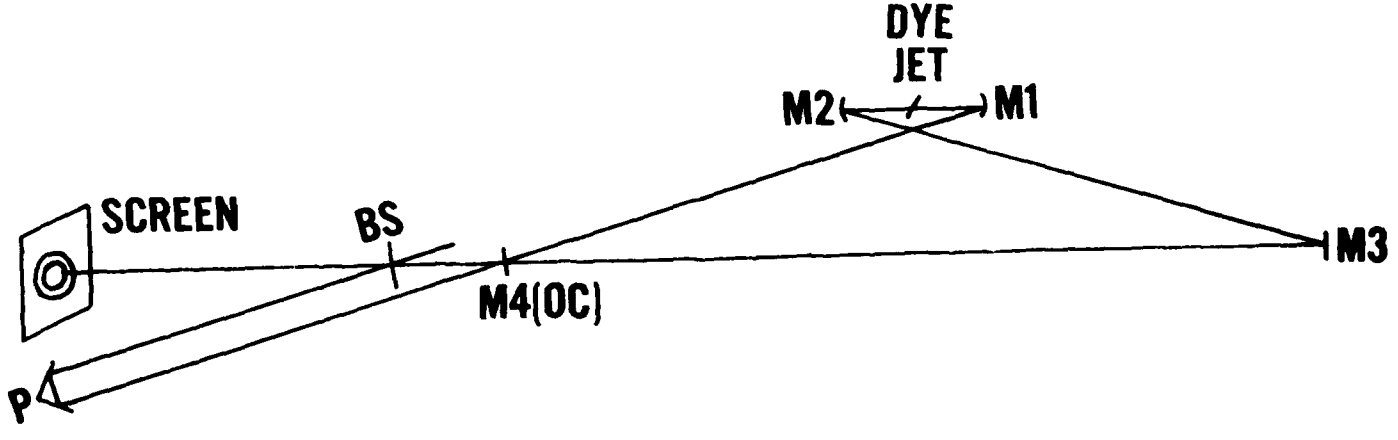
DYE
JET
M2
M1
SCREEN
BS
M4(OC)
M3
P

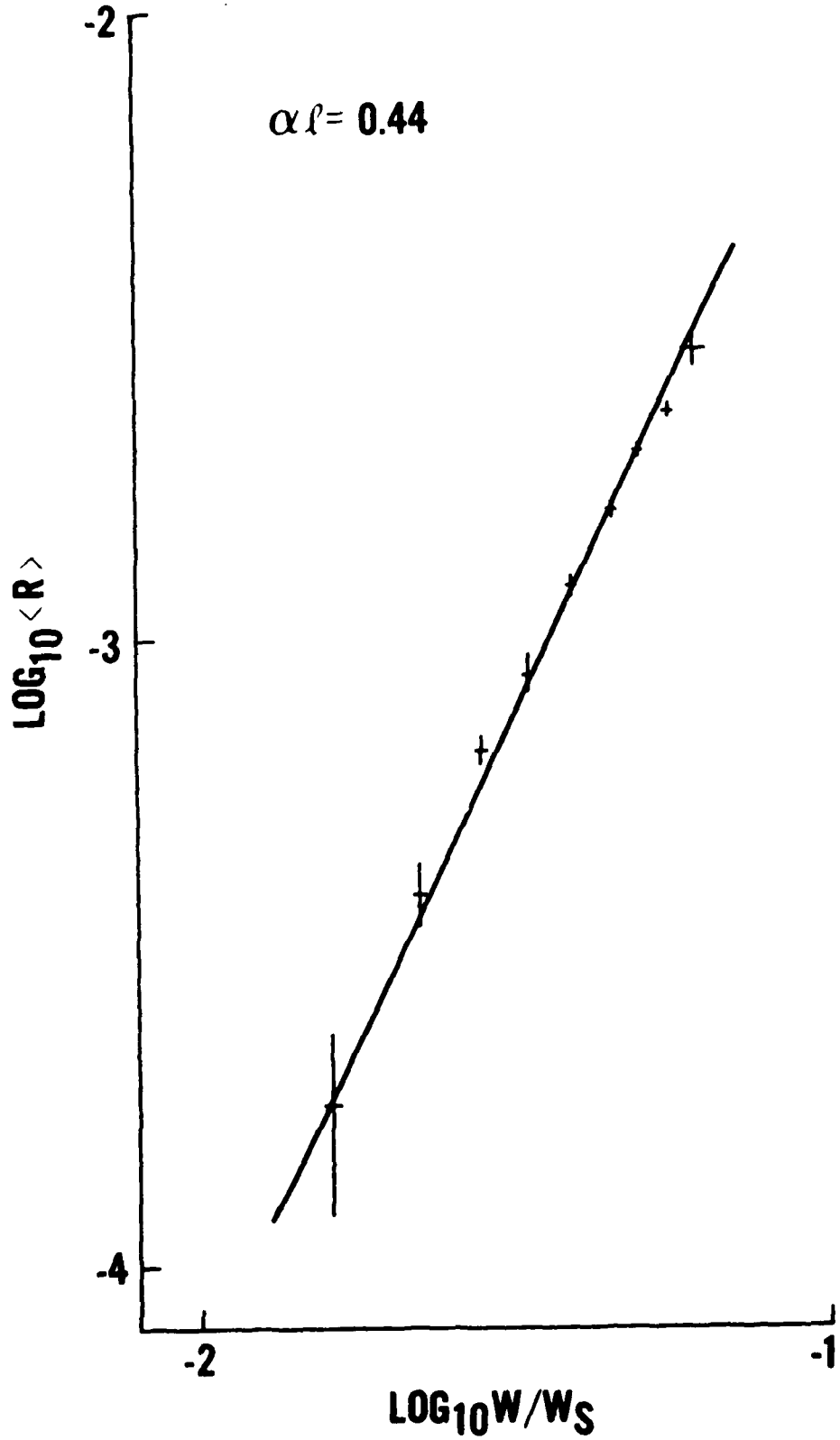
$\alpha\ell = 0.44$
-2
-3
-4
$LOG_{10}\langle R \rangle$
-2
-1
$LOG_{10}W/W_S$

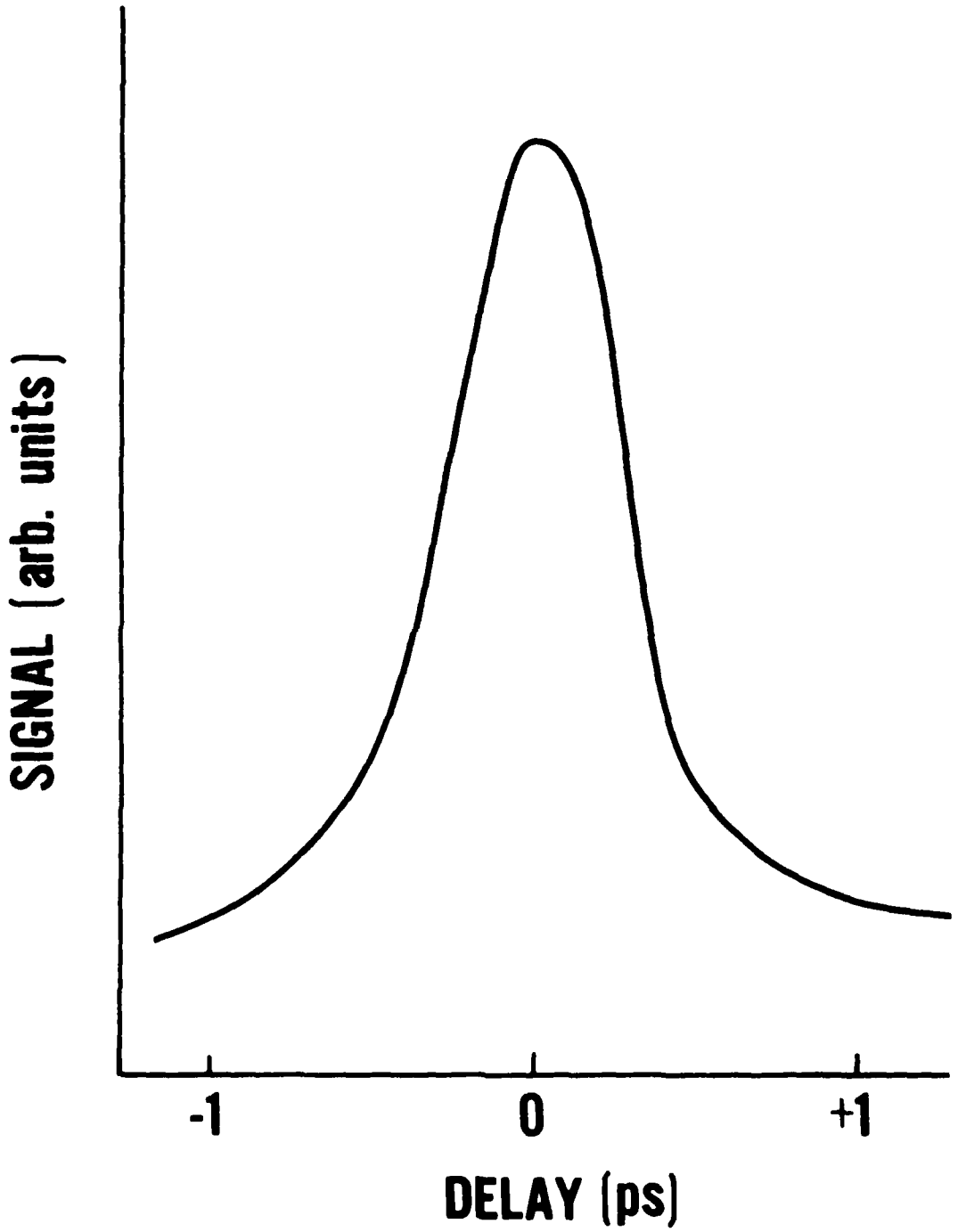
SIGNAL (arb. units)
-1
0
+1
DELAY (ps)

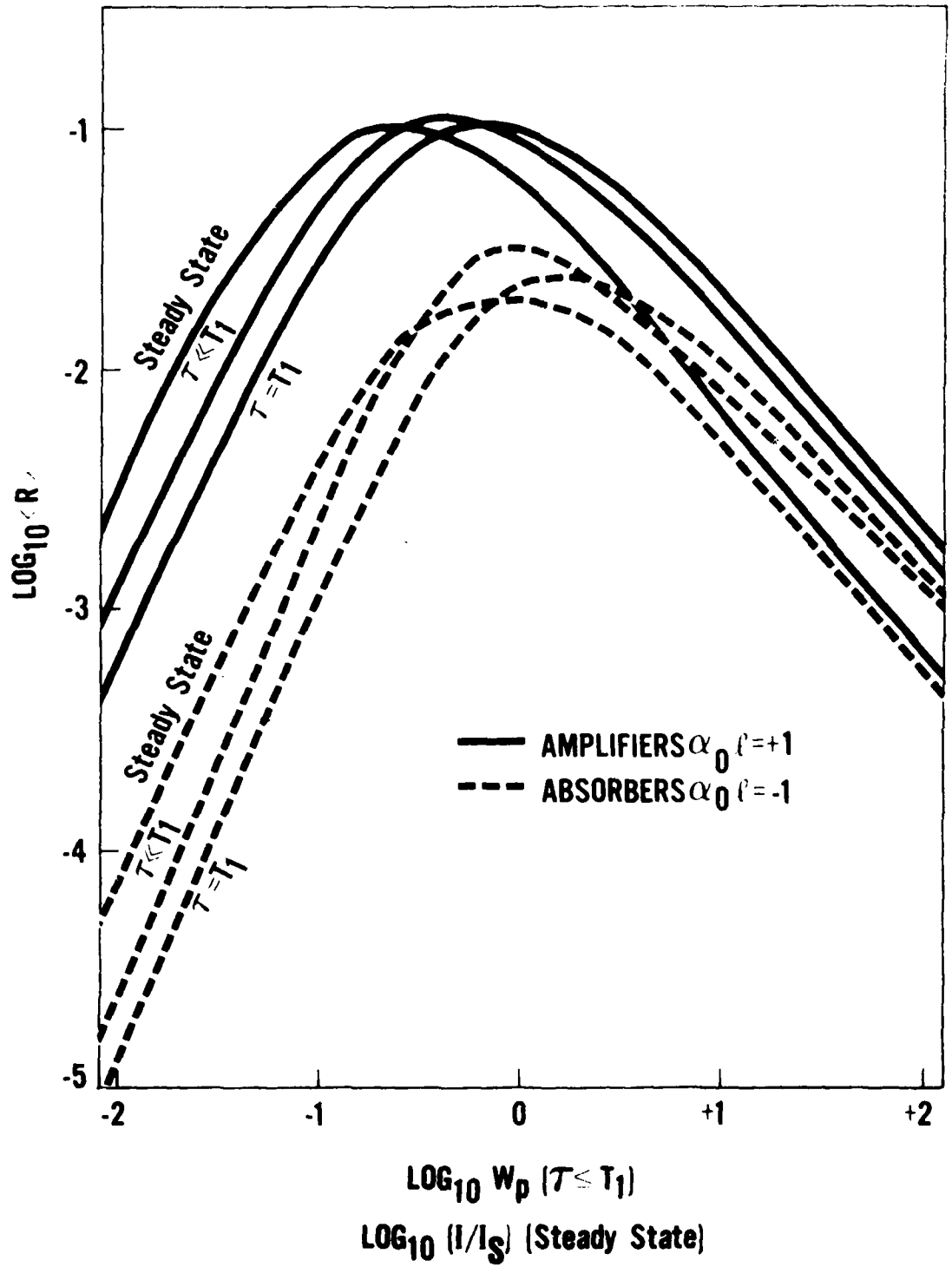
-1
-2
-3
-4
-5
Steady State
T≪T1
T≈T1
Steady State
T≪T1
T≈T1
AMPLIFIERS $\alpha_0 \ell = +1$
ABSORBERS $\alpha_0 \ell = -1$
-2
-1
0
+1
+2
$LOG_{10} W_p$ ($T \leq T_1$)
$LOG_{10} (I/I_S)$ (Steady State)

Intracavity pulse compression with glass: a new method of generating pulses shorter than 60 fsec

W. Dietel,* J. J. Fontaine,† and J.-C. Diels

Department of Physics, Center for Applied Quantum Electronics, North Texas State University, P.O. Box 5368, Denton, Texas 76203

Received September 24, 1982

The introduction of a glass prism in a ring dye laser is shown to provide simultaneous wavelength selection and pulse compression.

Significant progress has been made in the last decade in the generation of ultrashort dye-laser pulses. Subtle changes in cavity configuration resulted in dramatic changes in laser operation, which explains the somewhat erratic pace of progress in this field.

Pulses of 0.5-psec duration were generated in a linear configuration with two dye jets by Shank and Ippen.[1] The cavity loss modulation responsible for mode locking is obtained by saturation of the absorption in the dye diethyloxadicarbocyanine iodide (DODCI). The saturable absorber is flown through a jet located near the cavity end opposite the gain medium (Rh6G pumped by a cw argon laser). Pulse compression down to 0.3 psec was obtained with a pair of gratings.[2] By positioning the saturable absorber [diethylquinolyloxacarbocyanine iodide (DQOCI) in a dye cell] where the ultrashort laser pulse collides with itself at the cavity end mirror, Ruddock and Bradley[3] directly produced pulses of 0.3-psec duration. Diels *et al.*[4] choose a simpler configuration in which all the nonlinear elements (saturable absorber and gain medium) are mixed in the same dye jet. By a careful optimization of the dye mixture and cavity bandwidth (by eliminating all intracavity bandwidth-limiting elements and using carefully profiled mirror spectra), they obtained pulses as short as 120 fsec.[5] With a similar cavity configuration but using synchronous pumping and DQOCI, Mourou and Sizer produced pulses as short as 70 fsec (Ref. 6) with an exceptionally high conversion efficiency (10%). Instead of causing the pulse to collide with itself at the end of a linear cavity,[3] Fork *et al.*[7] used a ring-laser configuration in which the counterpropagating pulses collided in a thin saturable-absorber dye jet. The use of an absorbing-medium thickness as short as 10 μm resulted in a pulse duration of 90 fsec.[7] Shorter pulses (65 fsec) were reported[8] after optimization of the mirror spectra as in Ref. 5.

It is generally believed that the introduction of any dispersive intracavity element will produce a significant pulse broadening. Shank[8] reported an increase of pulse duration from 90 to 200 fsec by introduction of a microscope slide in the cavity. We demonstrate instead that, for a particular dye composition and wavelength, there is an optimal thickness of glass in the cavity that leads to the generation of the shortest pulses. For example, with a 2-mm thickness of BK7 inserted in our cavity, we recorded the second-order autocorrelation trace shown in Fig. 1, corresponding to a sech^2-shaped pulse of 53-fsec duration.

The laser configuration (Fig. 2) is similar to the one reported earlier by one of us.[9] All mirrors have maximum reflectivity coatings centered at 600 nm. A dispersive prism of BK7 or flint glass is used. Rotation and translation of the prism provide for independent control of the laser wavelength and the optical pathlength in glass, respectively. A standard coherent-radiation jet nozzle is used for the gain medium (100-μm thickness). The absorber jet is of a fanned-out type to provide for a thickness decreasing with distance from the nozzle, to a minimum of about 50 μm. It appears that, for our cavity configuration, the thickness of the jet is not of critical importance. The laser is pumped using all the lines of a Spectra-Physics Model 165-08

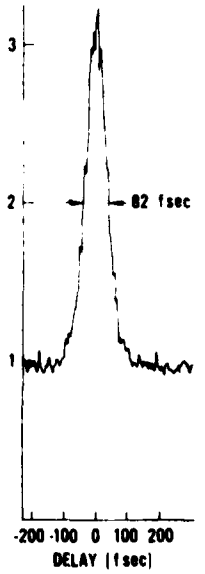

Fig. 1. Second-order autocorrelation of the pulse train, with peak-to-background ratio of 3 to 1. The autocorrelation width of 82 fsec corresponds to a sech^2 pulse duration of 53 fsec.

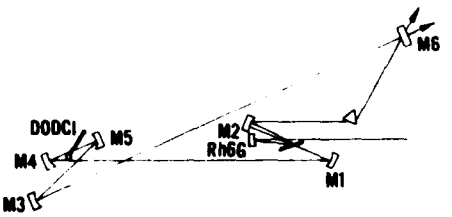

Fig. 2. Cavity configuration. The argon-laser pump mirror has a radius of curvature of 3 cm. The focusing mirrors around the amplifying and absorbing jets are, respectively, M1 and M2 (= 5 cm) and M4 and M5 (= 3 cm). The cavity mirror M3 has a radius of curvature of 1 m. The perimeter of the resonator is 3.6 m.

argon laser. The cw lasing threshold, in the absence of an absorber jet, is 80 mW. The DODCI solution with a concentration of 10^{-3} *M*/liter increased the threshold up to 4 W.

Two types of autocorrelator were used to monitor the laser output. The trace shown in Fig. 1 was recorded with an instrument using pellicle beam splitters to minimize the pathway in glass and collinear second-harmonic generation in a 0.3-mm-thick KDP crystal. The total pathway in glass, including the transmission through the output laser mirror, is 2.5 cm. Background-free autocorrelation traces, as in Fig. 3, were taken using polarizing beam splitters and type II second-harmonic generation in urea.[10] Two mutually delayed orthogonally polarized equal fractions of the laser beam are focused into the urea crystal. The measured autocorrelation width of 100 fsec (sech^2 pulse of 65 fsec FWHM) is remarkably short in view of the large thickness of glass (a total of 5 cm) traversed by the pulses between the laser and the second-harmonic-generating urea crystal. The measurement of Fig. 3 indicates that a resolution of tens of femtoseconds is possible for applications in time-resolved spectroscopy and fluorescence, or a resolution of the order of several micrometers for time-domain reflectometry[11] and optical imaging.[12]

The dependence of pulse duration on the optical pathway in glass is shown in Fig. 4. The pulse wavelength is maintained constant near 605 nm. For the measurement of Fig. 4, the prism of BK7 (n = 1.515) was replaced by a more-dispersive prism of flint glass (n = 1.62). It should be noted that qualitatively a similar pulse-width dependence can be measured at various wavelengths. However, the optimum glass thickness can vary by more than 1 order of magnitude with the laser wavelength. The wavelength dependence of the glass thickness at minimum pulse duration is not monotonic.[13] The various parameters of the laser (concentration, temperature, and age of the DODCI solution) have to be adjusted for each wavelength. If the dispersive prism is adjusted for minimum losses for each concentration of DODCI, a tuning curve (wavelength versus dye concentration) can be established.[13] The observed dependence is consistent with the recent observation[9] of *extracavity* pulse compression by passage of the pulse through a certain thickness of glass. The implication is that the nonlinearities in the absorbing (or amplifying) medium induce a downchirp.[9] Work is in progress to establish a theoretical model to match quantitatively the wavelength dependence of the observed downchirp. Pulses with such a frequency decreasing with time can be shortened by passage through a medium with normal dispersion (e.g., glass) since the training edge (seeing a smaller index) will catch up with the slower leading edge of the pulse. A compression by a factor of 1.5 was observed after transmission of 0.3-psec pulses through 17 cm of BK7

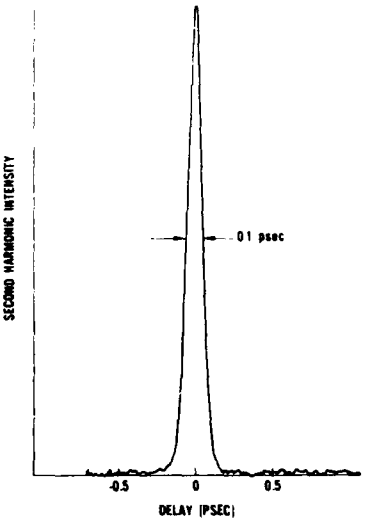

Fig. 3. Background-free autocorrelation recorded by type II second-harmonic generation in urea. The experimental arrangement is detailed in Ref. 10. The autocorrelation width of 100 fsec corresponds to a sech^2 pulse duration of 65 fsec. Spectral measurements indicate that the pulses are nearly bandwidth limited (6-nm bandwidth).

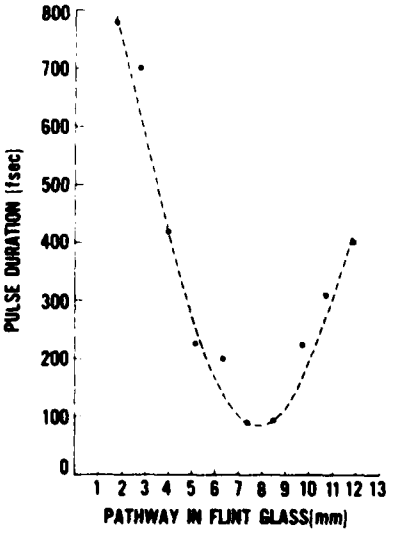

Fig. 4. Pulse duration versus thickness of glass (flint F2, n = 1.62) in the cavity for a particular wavelength (605 nm).

glass. However, the intensity autocorrelation of pulses of 0.15 psec remained unchanged, whereas a broadening by a factor of 2.3 was observed for 0.1-psec pulses.[9] Similar observations were reported by Mourou and Sizer for the synchronously passively mode-locked laser.[6] In the case of the cavity used in this work (Fig. 2), an intracavity pulse-compression mechanism takes place through successive passages through the absorbing and amplifying media (inducing down-frequency chirping) followed by transmission through glass.

In conclusion, we have demonstrated a laser that combines the above-mentioned intracavity compression mechanism with the stability of colliding pulse mode locking. The latter can be attributed to a stabilization mechanism introduced by a four-wave-mixing type of interaction in the absorber jet.[14]

This research was supported by the National Science Foundation under grant ECS-8119568 and by the Office of Naval Research.

* Permanent address, Sektion Physik, Friedrich-Schiller-Universität, Jena-69, German Democratic Republic.

† Permanent address, Ecole Nationale Supérieure des Arts et Industries de Strasbourg, Université Louis Pasteur, 5, rue de l'Université, 67000 Strasbourg, France.

References

1. C. V. Shank and E. P. Ippen, Appl. Phys. Lett. **24,** 373 (1974).
2. E. P. Ippen and C. V. Shank, Appl. Phys. Lett. **27,** 488 (1975).
3. I. S. Ruddock and D. J. Bradley, Appl. Phys. Lett. **29,** 296 (1976).
4. J.-C. Diels, E. W. Van Stryland, and G. Benedict, Opt. Commun. **25,** 93 (1978).
5. J.-C. Diels, E. W. Van Stryland, and J. Benedict, Opt. Commun. **25,** 93 (1978); J.-C. Diels, E. W. Van Stryland, and D. Gold, in *Proceedings of the First International Conference on Picosecond Phenomena* (Springer-Verlag, Berlin, 1978), p. 117; J.-C. Diels, J. Menders, and H. Sallaba, in *Proceedings of the Second International Conference on Picosecond Phenomena* (Springer-Verlag, Berlin, 1980), p. 41; J.-C. Diels, in *Proceedings of the Conference on Ultrashort Phenomena in Spectroscopy*, G. Wilhelmi, ed. (Jena U. Press, Jena, German Democratic Republic, 1981), p. 527.
6. G. A. Mourou and T. Sizer II, Opt. Commun. **41,** 47 (1982).
7. R. L. Fork, B. I. Greene, and C. V. Shank, Appl. Phys. Lett. **38,** 671 (1981).
8. C. V. Shank, presented at Twelfth International Quantum Electronics Conference, Munich, June 22, 1982.
9. W. Dietel, Dopel, D. Kuhlke, and B. Wilhelmi, Opt. Commun. (to be published); W. Dietel, D. Kuhlke, W. Rudolph, and B. Wilhelmi, in *Proceedings of Third International Conference on Picosecond Phenomena* (Springer-Verlag, Berlin, 1982).
10. J.-C. Diels, C. Y. Wang, and J. J. Fontaine, Photo-Opt. Instrum. Eng. **322,** 166 (1982).
11. J. J. Fontaine, J.-C. Diels, C. Y. Wang, and H. Sallaba, Opt. Lett. **6,** 405 (1981).
12. J.-C. Diels and J. J. Fontaine, "Imaging with short optical pulses," J. Opt. Lasers Eng. (to be published).
13. J. J. Fontaine, W. Dietel, and J.-C. Diels, "Tunable femtosecond dye laser," IEEE J. Quantum Electron. (to be published).
14. J.-C. Diels, J. J. Fontaine, I. C. McMichael, and C. Y. Wang, presented at the Twelfth International Quantum Electronics Conference, Munich, June 22, 1982); J.-C. Diels, I. C. McMichael, J. J. Fontaine, and C. Y. Wang, in *Proceedings of the Third Topical Meeting on Picosecond Phenomena* (Springer-Verlag, Berlin, 1982).

APPENDIX G

"Passive Mode-Locking Through Induced Total Reflection"

J.-C. Diels and C. Y. Wang*
Center for Applied Quantum ELectronics
North Texas State University
Denton, Texas 76203
(817) 788-2626

and

J. J. Fontaine
Groupe de Recherche et d'experimentation
en Photonique Appliquee
Universite Louis Pasteur
67000 Strasbourg, France

Abstract

Saturable absorption of the evanescent wave in total reflection is used as the nonlinearity responsible for passive mode-locking in a dye laser cavity.

*Optics Department of Tainjin (Tientsin)
University Tainjin (Tientsin)
The Peoples Republic of China

Passive Mode-Locking Through Induced Total Reflection

J.-C. Diels and C. Y. Wang*
Center for Applied Quantum ELectronics
North Texas State University
Denton, Texas 76203
(817) 788-2626

and

J. J. Fontaine
Groupe de Recherche et d'experimentation
en Photonique Appliquee
Universite Louis Pasteur
67000 Strasbourg, France

Summary

In passively mode-locked lasers, the cavity losses are modulated by a saturable absorber. Subpicosecond pulse generation[1,2,3] has been demonstrated for dye lasers passively mode-locked by a solution of diethyloxadicarbocyanine iodide (DODCI) and Malachite green. The saturable absorber was contained either in a jet[1,2] or in a thin cell.[3] The pulse duration appeared in most cases to be related to the fluid thickness. It has been suggested that degenerate four wave mixing (DFWM) took place within the cell[3] or the jet.[1] Theory shows that, in DFWM, a reflected signal pulse is always longer than the "probe" pulse by twice the medium thickness.[4] Therefore, in order to minimize the pulse lengthening process by DFWM, it is essential to confine the nonlinear medium in a thickness as short as possible. Fork et al. were able to build a dye jet as narrow at 10 μm. By using saturable absorption in the evanescent wave of a total reflection prism, we have reduced the interaction length to less than 1 μm. The intracavity laser beam was focused by two 5 cm radius of curvature mirrors, onto the reflecting interface, with an angle of

incidence of roughly 73°. A concentrated solution of DODCI is flown along the total reflection face of the prism. The prism and focusing optics are inserted in a ring dye laser cavity, in a position non symmetrical with respect to the amplifying Rh6G dye jet. In this configuration, mode-locking with colliding pulses in the absorber can be expected.[1] Mode-locked operation was observed, with equal intensity in the two counterpropagating beams. The mode-locked operation is dependent upon the flow condition. With a slow flow along the surface, the mode-locked changes successively from one pulse per cavity round-trip time, to two, then 4 pulses, then CW operation in a time of the order of 5 minutes. This indicates photodecomposition of the surface layer which has near zero velocity because of surface tension and fluid viscosity. The various laser operations resulting from different combinations of solvents and prism surface treatments will be described.

This work was supported by the Office of Naval Research and the National Science Foundation under grant ECS-8119568.

References

1. R. L. Fork, B. J. Greene and C. V. Shank, CLEO 81, Washington, June 1981.
2. J.-C. Diels, J. Menders and H. Sallabe, 2nd International Conference on Picosecond Phenomena, Cape Cod, Mass., June 1980; proceedings: Springer-Verlag, 41 (1980); J.-C. Diels, Ultrafast Phenomena in Spectroscopy, Reinhardsbrunn (Oct. 1980), proceedings, pp. 527-537 (1981).
3. I. S. Ruddock and D. J. Bradley, Appl. Phys. Lett. 29, 296 (1976).
4. J.-C. Diels, W. C. Wang, and H. Winful, to be published in Applied Physics (1981).